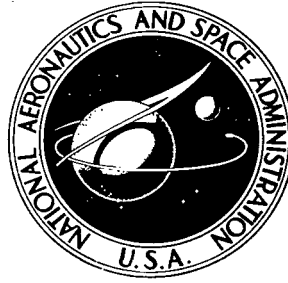


**NASA TECHNICAL NOTE**



**NASA TN D-7658**

C. I

**NASA TN D-7658**

**LOAN COPY: RETURN TO  
AFWL TECHNICAL LIBRARY  
KIRTLAND AFB, NM**



**PARAMETRIC THERMODYNAMIC ANALYSIS OF  
CLOSED-CYCLE GAS-LASER OPERATION IN SPACE**

*by Raymond K. Burns  
Lewis Research Center  
Cleveland, Ohio 44135*



**NATIONAL AERONAUTICS AND SPACE ADMINISTRATION • WASHINGTON, D. C. • MAY 1974**



0133623

1. Report No. NASA TND-7658	2. Government Accession No.	3. Recipient's Catalog No.	
4. Title and Subtitle PARAMETRIC THERMODYNAMIC ANALYSIS OF CLOSED-CYCLE GAS-LASER OPERATION IN SPACE		5. Report Date MAY 1974	6. Performing Organization Code
		8. Performing Organization Report No. E-7801	10. Work Unit No. 770-18
7. Author(s) Raymond K. Burns		11. Contract or Grant No.	
9. Performing Organization Name and Address Lewis Research Center National Aeronautics and Space Administration Cleveland, Ohio 44135		13. Type of Report and Period Covered Technical Note	
		14. Sponsoring Agency Code	
12. Sponsoring Agency Name and Address National Aeronautics and Space Administration Washington, D. C. 20546		15. Supplementary Notes	
16. Abstract Cycle efficiency and radiator area required were calculated for thermally and electrically pumped lasers operating in closed cycles with a compressor and the required heat exchangers. A thermally pumped laser included within a Brayton cycle was also analyzed. Performance of all components, including the laser, was parametrically varied. For the thermally pumped laser the cycle efficiencies range below 10 percent and are very sensitive to the high-pressure losses associated with the supersonic diffuser required at the laser cavity exit. The efficiencies predicted for the electrically pumped laser cycles range slightly higher, but radiator area also tends to be larger.			
17. Key Words (Suggested by Author(s)) Laser Space power system		18. Distribution Statement Unclassified - unlimited Category 16	
19. Security Classif. (of this report) Unclassified	20. Security Classif. (of this page) Unclassified	21. No. of Pages 59	22. Price* \$3.75

# PARAMETRIC THERMODYNAMIC ANALYSIS OF CLOSED-CYCLE GAS-LASER OPERATION IN SPACE

by Raymond K. Burns  
Lewis Research Center

## SUMMARY

An analysis of gas dynamic lasers operating in closed cycles was performed to predict thermodynamic cycle efficiency and radiator area required for rejection of waste heat to space. Thermally pumped and electrically pumped lasers were considered, with laser performance characterized in terms of nondimensional parameters.

Three types of closed cycles were considered. In two, the laser (thermally or electrically pumped) is included in a closed gas loop with a compressor and the heat exchangers required to return the gas flow at the laser exit to laser inlet conditions. In the third type of cycle, rather than using a separate system to power the laser cycle, the thermally pumped laser is included within a closed Brayton gas loop. In all cases, in addition to the laser performance parameters, the parameters describing the performance of the remainder of the cycle (and of the separate power system when required) were also independently varied.

The thermodynamic efficiency of a thermally pumped laser is improved by including it in a closed loop. But the large pressure losses associated with the diffuser, which is required to recompress the supersonic flow at the exit of the laser optical cavity, is a significant penalty on cycle performance. For the cases considered, the cycle efficiency ranges below 10 percent and is very sensitive to laser efficiency and to pressure losses. The results indicate that the maximum cycle efficiency would be obtained by a trade-off between laser efficiency and pressure losses.

The cycle efficiencies predicted for the electrically pumped laser cycle are in the same range or slightly higher than those for the thermally pumped laser. The required radiator area, however, tends to be larger because of the lower temperatures at which electric-discharge lasers operate. Since the operating temperature of electric-discharge lasers is usually near (or below) the space sink temperature, it appears necessary from the standpoint of closed-cycle operation to use a high-speed flow with an expansion at the laser inlet. In this way the lowest heat-rejection temperature (i. e., total temperature at the laser inlet) could be maintained at a level significantly above the static temperature in the laser optical cavity.

## INTRODUCTION

The production of high-power continuous-wave coherent radiation has become possible since the advent of the gas dynamic laser. Laser output powers in the tens of kilowatts have been achieved using CO<sub>2</sub>-N<sub>2</sub> thermally pumped lasers (e.g., ref. 1) and using CO<sub>2</sub>-N<sub>2</sub> electric-discharge gas lasers (e.g., ref. 2). Continuous, high-power output is made possible by the rapid removal of waste energy from the optical cavity by the gas flow, allowing the attainment of much higher power densities than can be achieved in static or slowly flowing gas lasers. For a thermally pumped gas dynamic laser, in addition to waste heat removal, the gas flow is used to create the population inversion by rapid expansion of an initially hot equilibrium gas through supersonic nozzles.

In mid-1971 the NASA Ad Hoc Laser Working Group was formed to examine possible future NASA uses of high-power lasers. The operation of high-power gas lasers in space was considered. The analysis of closed laser cycles which is presented herein was made as part of that investigation.

For long-term continuous operation in space, a high-power gas dynamic laser would have to be operated in a closed cycle in order to conserve the gas. In addition, for thermally pumped lasers, a closed cycle offers the potential for improved thermal efficiency (as discussed in ref. 3). In thermally pumped lasers the fraction of the total enthalpy of the entering gas which is removed in the laser cavity is small (~1 percent). A closed cycle would allow recovery of much of the remaining thermal energy. The extent of the improvement in efficiency would depend on the losses encountered in the closed cycle.

Closed cycle, thermally pumped laser systems have previously been analytically examined in references 3 to 5 in order to predict the cycle thermal efficiency. However, attention was focused on the thermodynamic limitations of the laser process, and losses in the rest of the cycle were neglected. In reference 3, the results of one calculation are presented, however, which do illustrate the significant effect of diffuser pressure losses in reducing the efficiency. Because of the typically high Mach numbers of the flow in thermally pumped gas dynamic lasers and the significant effect of diffuser losses on cycle efficiency, the supersonic diffuser was recognized as a significant technical problem.

In a space system, in addition to the cycle thermal efficiency, the weight and radiator area are also of prime importance. Therefore, this report examines the effects of the performance of the laser and of the other components in the cycle on both the cycle thermal efficiency and the required radiator area. The performance of the laser and that of the other components are represented parametrically.

## SCOPE OF ANALYSIS

This analysis was made to determine the effect of laser performance on closed-cycle operation, not to calculate laser performance. The parameters describing laser operation are varied independently, even though for any specific type of laser they may actually be interdependent. To add perspective, however, some laser performance parameters calculated at the NASA Ames Research Center for a carbon dioxide-nitrogen-helium ( $\text{CO}_2\text{-N}_2\text{-He}$ ) thermally pumped gas dynamic laser are included in appendix B. (All symbols used are defined in appendix A.) In each cycle analysis, the performance of the laser and that of the other components of the cycle are varied from currently attainable values into an optimistic region in order to indicate the potential for improvement of closed-cycle performance. Since laser performance is described parametrically, the cycle results should also be applicable to gas dynamic lasers of types other than  $\text{CO}_2\text{-N}_2$  lasers.

The analysis is divided into three sections. In the first two sections a thermally pumped gas dynamic laser is considered. First a closed cycle, referred to as the laser-compressor cycle, consisting of the laser and diffuser, a compressor, a recuperator, a waste heat exchanger, and a heat source is considered. Such an arrangement includes not only recuperation, but also the capability to vary the compressor inlet temperature. By reducing the laser exit gas temperature before compression, the mechanical problems and high compressor work associated with high compressor inlet temperatures are avoided. The compressor power for this cycle is assumed to be supplied by a separate power system.

In the second section a thermally pumped gas dynamic laser included in a closed Brayton cycle, referred to as a laser-Brayton cycle, is considered. After leaving the laser and diffuser, the gas is expanded through the turbine. The turbine provides the power required to drive the compressor and can also provide additional shaft power for some external use.

In the last section of the analysis an electric-discharge laser is considered. The closed cycle consists of the laser, a compressor, and a waste heat exchanger. The compressor work and laser electrical input are supplied by a separate power system.

The total temperature of the gas at the inlet to an electric-discharge laser is much lower than that at the inlet to a thermally pumped laser. Since the waste heat must be radiated to space in order to return the gas to the laser inlet temperature, this temperature must be at a reasonable level above the sink temperature to avoid excessively large radiator areas. In order to maintain the low translational temperature required in the laser optical cavity while keeping the cycle heat-rejection temperatures (laser inlet temperature) relatively high, it is assumed that the electric-discharge laser includes a nozzle at the inlet. The expansion ratio of the nozzle would be large enough to provide a sufficient reduction from the laser inlet temperature, but not large enough to

encounter large total pressure losses in the diffuser or in the laser where large amounts of heat are added to the gas. Electric-discharge lasers operating with high-speed flow have been reported in references 2, 6, and 7.

In calculating the radiator area, it was assumed in each case that the waste heat was rejected to a separate radiator loop. The effect of pumping power required for the radiator loop was not included. Also the effects on efficiency and radiator area of the coolant requirements for the laser optics and nozzles were not included.

### THERMALLY PUMPED GAS DYNAMIC LASER

In a thermally pumped laser, a hot equilibrium gas is rapidly expanded through a supersonic nozzle to create a population inversion between the upper and lower laser energy levels. Downstream of the nozzles the output radiant beam is produced as the gas flows through the optical cavity. Then, the gas flow is recompressed in a supersonic diffuser. In figure 1, a schematic of the laser nozzle, optical cavity, and diffuser is shown.

The variables indicated in figure 1 provide the definition of laser performance which is necessary for the closed-cycle thermodynamic calculations. For purposes of these calculations, it is advantageous to group the variables into a laser performance parameter

$$N_L \equiv \frac{Q_L}{\dot{m} C_p T_1} \quad (1)$$

and a laser pressure loss ratio

$$L_L = \frac{P_3}{P_1} \quad (2)$$

These parameters, the specific-heat ratio of the gas  $\gamma$ , and the laser inlet temperature  $T_1$  are used in the analysis to describe the laser performance.

For the cycle calculations, the ratio of diffuser exit temperature to nozzle inlet temperature is expressed as a function of the parameter  $N_L$ . Assuming that the only energy removed from the gas flow in the laser is that of the output beam power  $Q_L$  and that the specific heats of the gas at the laser inlet and exit are equal,

$$\frac{T_3}{T_1} = 1 - \frac{Q_L}{\dot{m}C_P T_1} = 1 - N_L \quad (3)$$

In the closed-cycle analysis, the parameter  $N_L$  is used to define the capacity flow rate  $\dot{m}C_P$  for a specified inlet temperature and output beam power. The higher the value of  $N_L$ , the lower the capacity flow rate for a given beam power, and hence the higher the closed-cycle thermal efficiency.

In addition to  $N_L$ , the pressure loss ratio  $L_L$  is an important measure of the laser performance with regard to the closed-cycle efficiency. The major part of these pressure losses occurs in the supersonic diffuser. The large expansion in the laser nozzle required for high laser performance results in high Mach number flow at the diffuser inlet. In addition to the diffuser losses, the pressure loss in the laser cavity is also considerable (ref. 3).

Since the pressure losses are a strong function of the flow Mach number, it appears desirable to reduce the Mach number in order to minimize the compressor power required to return the gas to the laser inlet pressure. However, a reduction in the nozzle expansion to reduce the Mach number could reduce the performance parameter  $N_L$  and hence increase capacity flow rate for a specified beam power  $Q_L$ . It is apparent that to minimize the compressor power or to maximize the closed-cycle efficiency, the laser design must be chosen for an optimum combination of  $N_L$  and  $L_L$ .

The values of  $N_L$  and  $L_L$  are not calculated in this analysis. They, the laser inlet temperature, and the specific-heat ratio of the gas are parametrically varied over a range of possible values. The closed-cycle performance as characterized by thermal efficiency and radiator size is calculated as a function of these laser parameters. For reference, some values of  $N_L$  calculated at the NASA Ames Research Center for a  $\text{CO}_2\text{-N}_2\text{-He}$  gas dynamic laser are given in appendix B.

### Laser-Compressor Cycle

The gas dynamic laser-compressor loop considered is shown schematically in figure 2. The temperature-entropy diagram is given in figure 3 with the state point numbering used in the analysis. The laser inlet and exit conditions are represented by states 1 and 2, respectively. The gas is compressed in the laser diffuser from point 2 to point 3. It then passes through a recuperator and is cooled to point 4. The gas is then further cooled as it passes through a waste heat exchanger where heat is rejected to a separate radiator loop. After being compressed from point 5 to point 6, the gas is heated in the recuperator to point 7 and then further heated in a heat-source heat exchanger to laser inlet conditions.

Procedure. - The thermodynamic cycle efficiency and total prime radiator area required for the cycle in figure 2 were calculated for a range of the component performance parameters. In addition to the laser parameter  $N_L$ , the laser inlet temperature  $T_1$ , the ratio of the compressor inlet to laser inlet temperature  $T_5/T_1$ , the total pressure loss ratio  $L_t$ , the recuperator effectiveness  $E_R$ , the compressor adiabatic efficiency  $\eta_C$ , and the efficiency of the power system which supplies the compressor power  $\eta_{PS}$  were varied parametrically. The laser pressure loss ratio  $L_L$  was included in the total pressure loss ratio  $L_t$ . For simplicity, it was assumed that the gas properties in the cycle are constant from the laser exit to the laser inlet. The specific-heat ratio of the gas was also parametrically varied.

The thermodynamic cycle efficiency is defined herein as the laser output power divided by the sum of the thermal inputs to the laser-compressor cycle and to the power system which supplies the compressor power. The total radiator area required is the sum of that required by the laser-compressor cycle and the power system. The prime radiator area required for the laser-compressor cycle was calculated and added to that of the power system, which was assumed parametrically in terms of area per unit of compressor power required. The total radiator area is presented in terms of area per unit of laser output power.

The parameters on which the radiator area depends other than those already mentioned were assigned reference values that are given in table I. The equations used in the cycle analysis are given in appendix C.

Results. - The thermal efficiency and specific prime radiator area were calculated (using equations in appendix C) for a range of cycle temperature ratio  $T_5/T_1$  and laser inlet temperature  $T_1$ . In figure 4, the specific radiator area is given as a function of cycle thermal efficiency for a range of  $L_t$  and  $N_L$ . The values of the remaining parameters used for these results are given in table I. The effects of variations in some of these remaining parameters is illustrated in some of the later figures.

In each of the curves in figure 4, there is a cycle temperature ratio for which the radiator area is at a minimum. At high values of cycle temperature ratio (high compressor inlet temperatures) the compressor power is high, and hence the power system radiator area is large. This area decreases as the cycle temperature ratio is decreased. At low cycle temperature ratios the heat-rejection temperatures in the laser-compressor loop are low, and therefore the laser-compressor loop radiator area is relatively large. As the cycle temperature ratio is increased, this radiator area decreases. At some intermediate value of temperature ratio the sum of the two radiator areas is at a minimum. For given values of  $L_t$  and  $N_L$ , the curves for different values of  $T_1$  approach each other for high values of cycle temperature ratio. This further indicates that at high cycle temperature ratios, the radiator area consists predominantly of the contribution from the power system. This contribution is a function of the compressor power (see eq. (C19)), which is shown by equation (C6) to be a func-

tion of the cycle temperature ratio. The effect of the power system specific radiator area  $(A_{R, P})_{PS}/W_C$  on these results is indicated in a later figure.

The primary information contained in the curves of figure 4 is the indication of the range of thermal efficiencies and radiator areas to be expected for a closed-loop gas dynamic laser. The effect of the total pressure loss parameter  $L_t$  on both thermal efficiency and radiator area is substantial. The values of  $L_t$  considered in figure 4 cover the range of interest. A value of  $L_t = 0.8$  is optimistic because of the large pressure losses in the laser optical cavity and in the laser diffuser. Values of  $L_t$  below 0.4 probably would not be of interest for a space system because of the comparatively low efficiency and large radiator areas.

For a  $CO_2-N_2-He$  thermally pumped gas dynamic laser a reasonable estimate of a value of  $L_t$  which could be achieved is 0.6 (appendix B). The range of  $N_L$  which is achievable with  $CO_2-N_2-He$  gas dynamic lasers is considered in figures 4(a) and (b); the value  $N_L = 0.015$  considered in figure 4(c) would probably be optimistic for  $CO_2-N_2-He$  lasers. The curves for  $L_t = 0.6$  in figures 4(a) and (b) are therefore representative (appendix B) of the potential performance of  $CO_2-N_2-He$  thermally pumped gas dynamic lasers.

The parameter  $N_L$  is approximately the ratio of the laser output power to the enthalpy of the gas flow input to the laser. For a  $CO_2-N_2-He$  laser this ratio is low, a few percent or less, since only a fraction (<10 percent) of the energy is in the vibrational levels of the molecules at the laser inlet. Of that energy, only part is in the laser upper energy level. And only part of that energy ultimately contributes to the output beam. The curves in figure 5 are not intended to be indicative of any particular type of gas dynamic laser but are included to further illustrate the significant effect on closed-loop performance of increases in the parameter  $N_L$ . These curves are for a laser inlet temperature of 1644 K (2500° F) and a total pressure loss parameter  $L_t$  of 0.6. The values of other parameters used are those in table I.

In figures 6 to 10 the effects of some of the other parameters are indicated. In each case the laser inlet temperature  $T_1$  was taken to be 1644 K (2500° F), the laser performance parameter  $N_L$  was assumed to be 0.01, and the total pressure loss parameter  $L_t$  was assumed to be 0.6. The values of parameters not specifically defined in each figure were taken to be the reference values in table I. Variations in specific-heat ratio and compressor adiabatic efficiency affect the compressor power, resulting in the variations in thermal efficiency and radiator area shown in figures 6 and 7.

As shown in figure 8, the effect of the laser-compressor loop recuperator effectiveness on both radiator area and thermal efficiency is largest at the low values of cycle temperature ratio. This follows from the fact that the amount of energy recuperated increases as the cycle temperature ratio decreases.

In figures 9 and 10 the effect of variation in the assumed values for power system efficiency and power system specific radiator area are shown. As discussed previously, the power system radiator contribution to the total radiator area is highest at the higher cycle temperature ratios. The effect of this is shown in the results given in figure 10.

### Laser-Brayton Cycle

The gas dynamic laser-Brayton cycles considered are shown schematically in figure 11. The laser and diffuser are included within a conventional closed Brayton loop between the heat-source heat exchanger and the turbine. A recuperator is included between the laser diffuser exit and the turbine to reduce the gas temperature to some specified turbine inlet condition. The cycle shown in figure 11(b) is simply a special case of that in figure 11(a) where the turbine inlet temperature is specified to be equal to the diffuser exit temperature.

The temperature-entropy diagram for the case of figure 11(a) is shown in figure 12. After being expanded through the turbine to point 5, the gas is cooled in the lower temperature recuperator to point 6 and then is further cooled to point 7 in the heat-sink heat exchanger. The heat rejected from the gas in the heat-sink heat exchanger is transferred to a separate radiator loop. After being compressed to point 8, the gas flows through the lower temperature and higher temperature recuperators to point 10. It is then heated back to laser inlet temperature in the heat-source heat exchanger.

Procedure. - As in the case of the laser-compressor cycle, the laser performance in the laser-Brayton cycle was described in terms of the parameters  $N_L$  and  $L_L$ . The effects of these performance parameters, and of those of the other components in the cycle, on thermodynamic efficiency and radiator area were investigated.

In this case the thermodynamic cycle efficiency is defined as the sum of the laser output power and any shaft power obtained from the Brayton cycle divided by the thermal input. The prime radiator area is presented in terms of area per unit of output power, where the output power is the sum of the laser and shaft output powers.

In addition to the laser parameter  $N_L$ , the ratio of output shaft power to laser power,  $P_{SH}/Q_L$ , the laser and turbine inlet temperatures  $T_1$  and  $T_4$ , the compressor pressure ratio  $P_8/P_7$ , the total pressure loss ratio  $L_t$ , the lower-temperature-recuperator effectiveness  $E_{RL}$ , and the turbine and compressor adiabatic efficiencies  $\eta_T$  and  $\eta_C$  were varied. Parameters which were assigned reference values are shown in table II. The equations used in the analysis are given in appendix C.

Results. - Using the equations in appendix C, the thermal efficiency and radiator area for the laser-Brayton closed cycle were determined for a range of laser and turbine inlet temperatures and for a range of the parameters  $N_L$  and  $L_t$ . In figure 13,

the total pressure loss parameter  $L_t$  is varied from 0.4 to 0.8 for two values of  $N_L$ . The laser inlet temperature was taken as 1644 K (2500<sup>o</sup> F), the turbine inlet temperature was assumed to be equal to the diffuser exit temperature (i. e. , the higher temperature recuperator was not included), and the shaft power was assumed to be zero. The values of parameters not specified were taken as the reference values in table II.

The compressor pressure ratio  $P_8/P_7$  and the cycle temperature ratio  $T_7/T_1$  (or compressor inlet temperature) vary along each of the curves in figure 13. The radiator area increases rapidly at each end of the curves as the compressor inlet temperature decreases and the heat-rejection temperatures approach the sink temperature.

The discontinuity exhibited in some of the curves in figure 13 results from the fact that as the compressor pressure ratio is increased the compressor exit temperature increases until it exceeds the turbine exit temperature and recuperation is not possible. The curves are intersections of solutions with recuperation (at lower pressure ratios) and without (at higher pressure ratios). The curves for  $L_t = 0.4$  do not show the discontinuity since the point at which recuperation becomes impossible does not occur within the range of pressure ratios considered (2 to 10). This point is further clarified in a later figure when the effect of the recuperator effectiveness is examined.

The ranges of  $L_t$  and  $N_L$  considered in figure 13 are the same as those considered for the laser-compressor closed loop in figure 4. As previously discussed, these ranges are of interest for the CO<sub>2</sub>-N<sub>2</sub>-He gas dynamic laser (also see appendix B).

As in the case of figure 4, the results in figure 13 show a substantial dependence on both  $N_L$  and  $L_t$ . The ranges of cycle efficiencies achieved are comparable for the two cases. However, detailed quantitative comparisons are difficult to make since the power conversion system efficiency and specific radiator area were fixed in the case of the laser-compressor cycle but are variable in the laser-Brayton cycle. (For example, in fig. 14 the effect of a change in laser inlet temperature (and consequently turbine inlet temperature) on the power conversion part of the system is included. However, in fig. 4, since the power conversion system is separate from the laser cycle, there is no effect of the laser inlet temperature on the power conversion system.)

By including the recuperator between the laser and turbine as shown in the schematic of figure 11(a), the turbine inlet temperature is reduced in order to relieve turbine cooling requirements while allowing the laser to operate at the higher temperatures necessary for its best performance. The effect on the thermal efficiency and radiator area of reducing the turbine inlet temperature is shown in figure 15. Laser inlet temperatures of 1367 and 1644 K (2000<sup>o</sup> and 2500<sup>o</sup> F) are considered, with turbine inlet temperatures down to 1144 K (1600<sup>o</sup> F). A different value of  $N_L$  is considered in each of figures 15(a) to (c). As the turbine inlet temperature is decreased, the heat-rejection temperatures of the cycle are reduced, resulting in the increase shown in radiator area. Also, the point on each curve where the radiator area is a minimum is shifted

to higher efficiency as the turbine inlet temperature is decreased.

Besides maintaining the gas flow to operate the laser in the closed loop, the turbomachinery can be used to generate additional power. If there is use for this power, it enters into the definition of thermal efficiency and specific radiator area as discussed in the previous section. The improvement in performance is shown in figure 16 for one case where gross shaft output power equals laser output power ( $P_{SH}/Q_L = 1.0$ ).

In the figures discussed to this point, the parameters not specified were taken as the reference values in table II. In figures 17 to 19 the effects of variations in turbine and compressor efficiencies and in low-temperature-recuperator effectiveness are shown. Variations in turbine and compressor efficiencies have more effect on radiator area than on efficiency. The effect is more significant at the lower turbine inlet temperatures. As shown in figure 19 the effect of variations in recuperator effectiveness from the reference value increases as the compressor pressure ratio is decreased and the difference between the inlet temperature on the two sides of the recuperator is consequently increased. Included in the figure is a solution for the nonrecuperated case to show that the discontinuity in the curves of previous figures corresponds to the intersection of solutions for the recuperated and nonrecuperated cycles.

## ELECTRIC-DISCHARGE GAS LASER

Figure 20 is a schematic showing the parameters of interest in this analysis for the electric-discharge gas laser (EDL). At station 1, a gas of specified temperature, pressure, and composition flows into the laser. This gas is subjected to an electric discharge to populate the laser upper energy level. By some means, the details of which are not of interest for these calculations, the upper level is populated and the lower energy level is depopulated to create an inversion. As the gas flows through an optical cavity, perpendicular to the optical axis, a laser output beam  $Q_L$  is produced.

If it is assumed that the only energy lost from the gas is that of the output beam  $Q_L$  and that the specific heat at the laser exit equals that at the inlet, the exit equilibrium temperature is

$$T_2 = T_1 + \frac{Q_E - Q_L}{\dot{m}C_P} \quad (4)$$

If we define a laser efficiency as

$$\eta_E \equiv \frac{Q_L}{Q_E} \quad (5)$$

and use the laser parameter defined in equation (1)

$$N_L = \frac{Q_L}{\dot{m}C_p T_1} \quad (1)$$

equation (4) becomes

$$T_2 = T_1 \left[ 1 + N_L \left( \frac{1 - \eta_E}{\eta_E} \right) \right] \quad (6)$$

The pressure ratio across the laser is denoted as  $L_L$ :

$$L_L = \frac{P_2}{P_1} \quad (7)$$

The pressure ratio  $L_L$ , the specific-heat ratio of the gas  $\gamma$ , the laser efficiency  $\eta_E$ , the parameter  $N_L$ , and the laser inlet temperature  $T_1$  are used in the cycle analysis to describe the laser performance. Each of these parameters is independently varied to determine its effect on the closed-cycle thermodynamic performance of the laser.

In a space system it would be necessary to keep the laser inlet temperature at a reasonable level above the sink temperature so that the radiator area does not become excessively large. However, this temperature level may be incompatible with the laser operation. It is therefore assumed that the laser indicated in figure 20 could include a nozzle through which the gas would be expanded to a desirably low translational temperature for the laser process. A diffuser would recompress the gas to state point 2 at the laser exit. The pressure loss ratio must therefore include the pressure losses of any nozzle and diffuser which might be included in the laser configuration.

The electric-discharge laser compressor cycles considered are shown in figure 21. The cycles contain a heat-sink heat exchanger and a compressor in addition to the laser. The waste heat is assumed to be rejected to a separate radiator loop. The compressor power and the electrical power input to the laser are assumed to be delivered by a power system with an assigned efficiency and a specific radiator area. The overall thermal efficiency and radiator areas are calculated for each configuration for a range of pressure loss ratios, laser inlet temperatures, and laser performance parameters  $\eta_E$  and  $N_L$ .

## Procedure

The cycle efficiency of the electric-discharge laser-compressor cycles is defined as the laser output power divided by the thermal input to the power system which supplies the electrical power and compressor power required by the laser compressor cycle. As shown in appendix C the cycle efficiency can be expressed as a function of the laser parameters  $\eta_E$  and  $N_L$ , the specific-heat ratio of the gas  $\gamma$ , the total pressure loss ratio  $L_t$ , the adiabatic efficiency of the compressor  $\eta_C$ , and the efficiency of the power system. It was assumed for simplicity that the efficiency of the power system is the same for supplying electrical power as for supplying compressor power.

The prime radiator area per unit of laser output power for the laser-compressor cycle depends on the absolute temperature level as well as on the parameters affecting the efficiency. The laser inlet temperature was used to define the temperature level. The power system radiator area was added to this radiator area, and the total is presented. The power system radiator area was determined by assuming values for the power system radiator area per unit of electrical power and per unit of compressor power and then multiplying these values by the required electrical power and compressor power, respectively. This power system specific radiator area was parametrically varied.

The parameters which were not varied were assigned values as shown in table III. The equations used in the cycle analysis are given in appendix C.

## Results

The closed-cycle thermal efficiency in the limiting case of zero pressure losses is the product of the laser efficiency  $\eta_E$  and the efficiency of the power system which supplies the laser electrical input. In an actual case the efficiency is lower because of the compressor power required. In figure 22 the cycle thermal efficiency for loop configuration A is shown for a range of  $\eta_E$ ,  $N_L$ , and  $L_t$ . As  $L_t$  is decreased (increased pressure losses) and  $N_L$  is decreased (increased capacity flow rate for a given laser output power and inlet temperature), the compressor power is increased and the cycle efficiency is consequently reduced.

Since the compressor inlet temperature and consequently the compressor work are lower for loop configuration B than for configuration A for the same values of  $\eta_E$ ,  $N_L$ , and  $L_t$ , the cycle efficiency will be higher. This difference is shown in figure 23.

The values of parameters not specified in figures 22 and 23 were taken as the reference values in table III. Since, for the approximations made, the efficiency of both loop configurations is directly proportional to the efficiency of the power system, the

effect on the results shown in figures 22 and 23 of changing the power system efficiency from the 25 percent reference value used is easily determined.

As stated previously the parameters  $\eta_E$  and  $N_L$  are used in the cycle analysis to describe the laser performance. Neither of these parameters is calculated in this analysis but each is independently varied over a range of possible values. Actually, the parameters  $\eta_E$  and  $N_L$  are not independent, and there probably are combinations of these parameters which are not possible or would not be desirable in a closed loop. The gas is heated as it flows through the laser by the energy difference between the electrical input and the laser output. The rise in translational temperature in the laser cavity must be limited in order to avoid a degradation in the population inversion caused by increased population of the lower energy levels. The gas flow rate must be high enough to prevent such a deleterious temperature rise. For a given gas composition, laser inlet total temperature, and laser output power, this condition limits the possible range of the parameter  $N_L$  for a particular value of  $\eta_E$ . This limit depends on the particular laser design and is not further considered herein.

If we assume for a moment that a laser can be operated with a particular combination of  $\eta_E$  and  $N_L$ , a consideration influencing the desirability of that combination of parameters in a closed loop is the total temperature rise in the gas from the laser inlet to the exit. The ratio of laser exit to inlet total temperature varies linearly with  $N_L$ , and the rate of increase with increasing  $N_L$  depends on  $\eta_E$  (eq. (6)) as shown in figure 24. As shown in the figure the range of  $N_L$  might have to be restricted in order to limit the total gas temperature at the laser exit because of materials considerations. (The temperature rise indicated in figure 24 is the equilibrium total temperature rise, which would be larger than the translational temperature rise in the laser cavity discussed previously.)

In the case of loop configuration A (fig. 21) the compressor exit temperature is the maximum loop temperature. The ratio of that temperature to the laser inlet temperature is shown in figure 25 for a range of  $\eta_E$ ,  $N_L$ , and  $L_t$ .

The heat rejected from loop configuration A reduces the gas temperature from the compressor exit to the laser inlet. These temperatures (fig. 25) were used in equations (C50), (C51), and (C17) to calculate the prime specific radiator area required for this heat rejection. Adding the power system radiator area (eq. (C52)) to this value yields the total radiator size shown in figure 26 for two laser inlet temperatures. The values of parameters not specified were taken as the reference values in table III. As would be expected, the radiator area is lower for higher values of laser efficiency (lower heat-rejection loads). Also, for a particular value of  $\eta_E$  and  $L_t$ , the specific radiator area is reduced as the parameter  $N_L$  is increased. For a fixed value of laser inlet temperature, an increase in  $N_L$  means a reduction in capacity flow rate for a particular laser output power. This reduced flow rate results in a reduction in the ratio

of compressor power to laser output power, which in turn reduces the heat rejection and hence the radiator size for both the laser loop and the power system. Also an increase in  $N_L$  results in an increase in the temperature of heat rejection (fig. 25) and hence a decrease in radiator area.

The advantages in increasing the laser inlet temperature and consequently the heat-rejection temperatures in order to reduce radiator area are shown by a comparison of figures 26(a) and (b). Increasing the laser temperature while maintaining the lower translational temperature required for laser operation might be accomplished by expanding the flow in a nozzle before it enters the laser optical cavity.

The pressure loss parameter  $L_t$  was held at 0.8 in figure 26. The effect of variations in pressure loss is shown in figure 27 for loop configuration A. A decrease in pressure loss reduces the compressor power and hence the radiator area in both the laser loop and the power system. The effect decreases as  $N_L$  is increased (i.e., as the capacity flow rate is decreased for fixed laser inlet temperature and laser output power).

As shown in figure 23 the cycle thermal efficiency for loop configuration B is higher than that for configuration A because of its lower compressor inlet temperature and therefore lower compressor power. Therefore, the radiator heat-rejection load is lower for configuration B than for A. However, for the same laser inlet temperature, the heat-rejection temperature range for configuration B extends to lower temperatures than it does for configuration A. (The temperature of the heat-sink heat-exchanger exit gas in configuration B is less than the laser inlet temperature.) As shown in figure 28 the overall result is higher total radiator area for configuration B over most of the range of parameters shown.

The laser loop configurations in figure 21 were considered only as examples. As discussed, the efficiency of configuration B is higher than that of A; however, the radiator area required by configuration B is larger. A compromise configuration might include two waste heat exchangers: one to cool the working gas from the laser exit temperature before compression, and the other to cool the gas at the compressor exit back to laser inlet conditions. We assumed that the gas is cooled in the first waste heat exchanger so that the compressor inlet temperature equals the laser inlet temperature. With this assumption the efficiency and radiator area requirement of such a configuration were calculated for  $T_1 = 311 \text{ K}$  ( $560^\circ \text{ F}$ ),  $N_L = 0.1$ ,  $\eta_E = 0.3$ , and  $L_t = 0.8$ . The 6.1 percent efficiency and  $11.3\text{-m}^2/\text{kW}$  ( $122\text{-ft}^2/\text{kW}$ ) radiator area for this case are between the values for the two cycle configurations considered in figures 23 and 28.

In figure 29, the effect of the assumed value of power system specific radiator area on the total radiator area is illustrated. Although not shown in figure 29, the effect of power system specific radiator area would decrease for increased laser efficiency  $\eta_E$  because of the lower electrical input required at higher efficiency.

## CONCLUDING REMARKS

Use of a closed cycle for a thermally pumped gas dynamic laser improves the efficiency over that of an open cycle by conserving part of the thermal energy of the gas flow at the diffuser exit. However, for the cases which correspond to the expected performance of a  $\text{CO}_2\text{-N}_2$  laser, the cycle efficiencies presented are less than 10 percent. This low efficiency results from the low value of the laser performance parameter  $N_L$  and the high total pressure losses, both of which result in a high ratio of compressor power to laser output. A low value of  $N_L$  is inherent in the  $\text{CO}_2\text{-N}_2$  thermally pumped laser. (Only a small fraction of the total enthalpy of the flow inlet to the laser can be in that vibration energy level which is the laser upper energy level.) The high pressure losses result from the large laser nozzle expansion required to create the population inversion. The large expansion results in high Mach number flow, which in turn results in substantial losses in the supersonic diffuser and in the laser cavity (where waste heat is added to the supersonic flow).

The laser-Brayton cycle which was considered results in higher thermal efficiency and lower specific radiator area than the laser-compressor cycle considered. The performance of both cycles is highly dependent on the values of  $N_L$  and  $L_t$ . The radiator areas predicted for the laser-Brayton cycle show a stronger dependence on pressure loss and laser inlet temperature than those for the laser-compressor cycle.

If it is assumed that the laser performance parameter  $N_L$  remains the same, an increase in laser inlet temperature improves the closed-cycle performance. In the laser-Brayton cycle when the laser-diffuser exit temperature is raised to a level above which turbine cooling becomes a problem, a recuperator inserted between the diffuser and turbine can be used to reduce the turbine inlet temperature. Thus, the radiator area is increased over what it would be without the reduction in turbine inlet temperature. In an actual case an increase in laser inlet temperature could result in an improvement in laser performance  $N_L$ . So cycle performance might be improved by using the recuperator to hold turbine inlet temperature constant while increasing laser inlet temperature.

An electric-discharge gas laser has the advantage over thermally pumped lasers in a closed loop of operating at lower total temperatures and with lower pressure losses. At lower cycle maximum temperatures, the heat loss, cooling, and materials problems would be lessened. The thermal efficiencies predicted for the electric-discharge laser cycle are in the same range or slightly higher than those for the thermally pumped laser. However, since electric-discharge lasers operate at static gas temperatures near (or below) the space sink temperature, it appears necessary to use a high-speed flow with an expansion at the laser inlet. The results presented show that if this method is used to maintain the laser inlet total temperature several hundred degrees above the sink

temperature, the radiator area required can be reduced to the range predicted for the thermally pumped laser cycles.

Lewis Research Center,  
National Aeronautics and Space Administration,  
Cleveland, Ohio, January 21, 1974,  
770-18.

## APPENDIX A

### SYMBOLS

$A_{R, P}$	prime radiator area
$(A_{R, P})_{LC}$	prime radiator area for laser cycle
$(A_{R, P})_{PS}$	prime radiator area for power system
$(A_{R, P})_T$	total prime radiator area
$C_P$	specific heat at constant pressure
$C_R$	heat-sink heat-exchanger capacity rate ratio, $(\dot{m}C_P)_G / (\dot{m}C_P)_L$
$E_R$	recuperator effectiveness
$E_{RH}$	effectiveness of higher temperature recuperator
$E_{RL}$	effectiveness of lower temperature recuperator
$E_S$	effectiveness of heat-sink heat exchanger
$L_L$	laser pressure loss ratio, eq. (2) or (7)
$L_t$	total pressure loss ratio, eq. (C3), (C21), or (C40)
$\dot{m}$	mass flow rate
$N_L$	laser performance parameter, eq. (1)
$P$	total pressure
$P_{SH}$	gross shaft power
$Q_E$	electrical input power for electric-discharge laser
$Q_L$	laser output power
$T$	total temperature
$T_S$	sink temperature
$W_C$	compressor power
$W_T$	turbine power
$\gamma$	ratio of specific heats
$\epsilon_r$	radiator emissivity
$\eta_C$	compressor adiabatic efficiency

$\eta_{cy}$  cycle thermal efficiency  
 $\eta_E$  electric-discharge laser efficiency, eq. (5)  
 $\eta_{PS}$  power system efficiency  
 $\eta_T$  turbine adiabatic efficiency

**Subscripts:**

ex exit  
G gas  
in inlet  
L coolant

## APPENDIX B

### PERFORMANCE PREDICTION FOR CO<sub>2</sub>-N<sub>2</sub>-He GAS DYNAMIC LASER AND DIFFUSER

As a guide for the selection of the ranges of laser performance parameters used in the closed-cycle analyses for the thermally pumped gas dynamic laser, the laser performance was analytically predicted by the Fluid Mechanics Branch at the Ames Research Center. Some of the results are given in table IV for several laser output power levels, for nozzle area ratios of 6.0 and 11.9, and for laser inlet temperatures of 1367 and 1644 K (2000<sup>o</sup> and 2500<sup>o</sup> F). (The performance parameter given in table IV is slightly different than that used in the cycle analysis in that the total enthalpy at the laser inlet is used rather than the product of specific heat and total temperature.) The results in table IV were calculated by using Anderson's gain theory (ref. 8) and a modification of Rigrod's power theory (ref. 9). The results of these theoretical methods and experiment are compared in references 10 and 11. In calculating the results in table IV the mirror absorptivity was assumed to be 2 percent and the distance between cavity mirrors was assumed to be 70 centimeters for 10 kilowatts, 2 meters for 100 kilowatts, and 8 meters for 1 megawatt of laser output power. The results given are not necessarily optimum but are presented as examples. The variation in laser performance as a function of temperature, pressure, and composition is examined in references 10 to 12.

Table IV demonstrates that laser performance  $N_L$  is significantly improved by raising the inlet temperature from 1367 to 1644 K (2000<sup>o</sup> to 2500<sup>o</sup> F) or by raising the nozzle area ratio from 6.0 to 11.9. For a nozzle area ratio of 6.0 the Mach number varies from about 3.2 to 3.5 for the compositions shown in table IV. For an area ratio of 11.9 the Mach number is slightly above 4.0.

The total pressure losses in the laser cavity are predicted to be about 15 percent for the cases shown in table IV. The total pressure losses in the supersonic diffuser strongly depend on the diffuser inlet Mach number.

In figure 30 some experimental results are given to serve as a guide to estimate the total pressure recovery which might be attained in the diffuser. The symbols shown from reference 13 are experimental data from supersonic inlet systems with boundary layer control. The dashed line is obtained from experimental data given in reference 14 at a lower stagnation pressure by extrapolating to the  $3.0 \times 10^6$ -N/m<sup>2</sup> (30-atm) pressure considered in table IV.

An important consideration in diffuser performance is the aspect ratio (ratio of height to width) at the diffuser entrance. For the data from reference 14 the aspect ratio is 1.0; for typical thermally pumped gas dynamic lasers the aspect ratio is much lower. This would increase the influence of the boundary layer and make it difficult to attain the performance indicated by the dashed line in figure 30.

When the dashed curve in figure 30 is used as an estimate of diffuser performance, the pressure recovery for a Mach number of 3 would be about 0.67. Using the 15 percent total pressure loss estimated for the conditions in table IV results in an overall pressure ratio for the laser-diffuser combination ( $L_L$  of eq. (2)) of about 0.57. For a Mach number of 4 the diffuser pressure recovery would be about 0.44. Together with the 15 percent loss in the laser, this results in an overall pressure recovery  $L_L$  of about 0.37. It can be seen that the losses increase rapidly with Mach number.

From table IV, it is seen that the laser performance is predicted to improve significantly by changing the nozzle area ratio from 6.0 to 11.9. However, since this change also significantly increases the pressure losses, it follows that for optimum closed-cycle performance, a compromise between laser performance  $N_L$  and pressure losses  $L_L$  is necessary.

## APPENDIX C

### CYCLE ANALYSIS EQUATIONS FOR THERMALLY PUMPED

#### GAS DYNAMIC LASER CYCLES

##### Laser-Compressor Cycle

For a particular laser, the exit conditions (state point 3) can be expressed as a function of the inlet conditions and the laser parameters  $N_L$  and  $L_L$ :

$$\frac{T_3}{T_1} = 1 - N_L \quad (C1)$$

$$\frac{P_3}{P_1} = L_L \quad (C2)$$

In terms of the pressure losses in the laser and in the rest of the loop, the compressor pressure ratio is

$$\frac{P_6}{P_5} = \frac{1}{L L_L} = \frac{1}{L_t} \quad (C3)$$

where  $L$  is the loop pressure loss ratio defined as

$$L \equiv \left( \frac{P_1}{P_6} \right) \left( \frac{P_5}{P_3} \right) \quad (C4)$$

If perfect-gas relations are assumed, the compressor power required in the loop is

$$W_C = \frac{\dot{m} C_P T_{in}}{\eta_C} \left[ \left( \frac{P_{ex}}{P_{in}} \right)^{(\gamma-1)/\gamma} - 1 \right] \quad (C5)$$

Using this expression and the definition of the laser performance parameter  $N_L$  yields the ratio of compressor power to laser output power

$$\frac{W_C}{Q_L} = \frac{1}{N_L \eta_C} \left( \frac{T_5}{T_1} \right) \left[ \left( \frac{1}{L_t} \right)^{(\gamma-1)/\gamma} - 1 \right] \quad (C6)$$

The compressor exit temperature is

$$T_6 = T_5 + \frac{W_C}{\dot{m} C_P} \quad (C7)$$

Using the definition of  $N_L$  (eq. (1)) yields

$$T_6 = T_5 + N_L T_1 \left( \frac{W_C}{Q_L} \right) \quad (C8)$$

The remaining cycle temperatures are calculated by using

$$T_7 = T_6 + E_R (T_3 - T_6) \quad (C9)$$

$$T_4 = T_3 - E_R (T_3 - T_6) \quad (C10)$$

The thermal efficiency, defined as laser output power divided by total thermal input, is symbolically

$$\eta_{cy} = \frac{Q_L}{\dot{m} C_P (T_1 - T_7) + \frac{W_C}{\eta_{PS}}} \quad (C11)$$

where  $\eta_{PS}$  is the efficiency of the power system which supplies the compressor power. Thermal efficiency can be written in terms of  $N_L$  as

$$\eta_{cy} = \frac{1}{\frac{1}{N_L} \left( 1 - \frac{T_7}{T_1} \right) + \frac{1}{\eta_{PS}} \left( \frac{W_C}{Q_L} \right)} \quad (C12)$$

The temperature ratio  $T_7/T_1$  can be written as follows by using equations (1), (C8), and (C9):

$$\frac{T_7}{T_1} = (1 - E_R) \left[ \frac{T_5}{T_1} + N_L \left( \frac{W_C}{Q_L} \right) \right] + E_R(1 - N_L) \quad (C13)$$

Combining equations (C6), (C12), and (C13) results in an expression for the cycle thermal efficiency as a function of the cycle temperature ratio  $T_5/T_1$ ,

$$\eta_{cy} = \frac{N_L}{E_R N_L + (1 - E_R) \left( 1 - \frac{T_5}{T_1} \right) + \left[ \frac{1}{\eta_{PS}} - (1 - E_R) \right] \frac{1}{\eta_C} \left( \frac{T_5}{T_1} \right) \left[ \left( \frac{1}{L_t} \right)^{(\gamma-1)/\gamma} - 1 \right]} \quad (C14)$$

It is assumed that the heat rejection between state points 4 and 5 is to a separate radiator loop, as shown in figure 2. The radiator fluid inlet and exit temperatures are given by

$$T_{5,L} = \frac{1}{E_S} [T_5 - (1 - E_S)T_4] \quad (C15)$$

$$T_{4,L} = T_{5,L} + C_R(T_4 - T_5) \quad (C16)$$

The prime radiator area is calculated, by using reference 15, as

$$A_{R,P} = \frac{\dot{m}C_P}{4C_R\epsilon_r\sigma T_S^3} \left\{ \ln \left[ \frac{(T_{L,in} - T_S)(T_{L,ex} + T_S)}{(T_{L,ex} - T_S)(T_{L,in} + T_S)} \right] - 2 \left[ \tan^{-1} \left( \frac{T_{L,in}}{T_S} \right) - \tan^{-1} \left( \frac{T_{L,ex}}{T_S} \right) \right] \right\} \quad (C17)$$

where  $T_{L,in}$  and  $T_{L,ex}$  are the coolant temperatures at the inlet and exit of the radiator. The temperature difference between the radiator surface and the radiator coolant is neglected. Using the definition of  $N_L$  yields the specific prime radiator area for the laser-compressor loop

$$\frac{(A_{R,P})_{LC}}{Q_L} = \frac{1}{T_1 N_L C_R 4 \epsilon_r \sigma T_S^3} \left\{ \ln \left[ \frac{(T_{4,L} - T_S)(T_{5,L} + T_S)}{(T_{5,L} - T_S)(T_{4,L} + T_S)} \right] - 2 \left[ \tan^{-1} \left( \frac{T_{4,L}}{T_S} \right) - \tan^{-1} \left( \frac{T_{5,L}}{T_S} \right) \right] \right\} \quad (C18)$$

From equations (1), (C6), (C8), (C10), (C15), and (C16), the coolant temperatures can be expressed as a function of the temperature ratio  $T_{5,L}/T_1$  and  $T_1$ . The radiator area is a function not only of the cycle temperature ratio, but also of the laser inlet temperature.

In addition to the radiator area required for heat rejection from the laser-compressor loop, the radiator area for the power system which supplies the compressor work must be calculated. This is

$$\frac{(A_{R,P})_{PS}}{Q_L} = \frac{(A_{R,P})_{PS}}{W_C} \left( \frac{W_C}{Q_L} \right) \quad (C19)$$

where  $W_C/Q_L$  is given by equation (C6). The power system specific prime radiator area  $(A_{R,P})_{PS}/W_C$  has been assigned a reference value (see table I) for this analysis of  $0.93 \text{ m}^2/\text{kW}$  ( $10 \text{ ft}^2/\text{kW}$ ), which could be achieved with an advanced Brayton system. The total specific prime radiator area is therefore

$$\frac{A_{R,P}}{Q_L} = \frac{(A_{R,P})_{LC}}{Q_L} + \frac{(A_{R,P})_{PS}}{Q_L} \quad (C20)$$

### Laser-Brayton Cycle

As in the case of the laser-compressor loop, the laser exit conditions (state point 3) are expressed in terms of the inlet conditions, and the laser parameters  $N_L$  and  $L_L$  by equations (C1) and (C2). In addition to the laser inlet conditions and the turbine inlet temperature  $T_4$ , the gross shaft power output of the turbomachinery  $P_{SH}$  and the compressor pressure ratio  $P_8/P_7$  are specified. The rest of the state points in the cycle, the thermal efficiency, and radiator area are then calculated. Because of the constraints introduced by the laser, the analysis is somewhat different than that ordinarily

used for Brayton cycles.

In terms of the specified compressor pressure ratio, the turbine pressure ratio is

$$\frac{P_4}{P_5} = L L_L \frac{P_8}{P_7} = L_t \frac{P_8}{P_7} \quad (C21)$$

where  $L$  is the loop pressure loss ratio defined

$$L \equiv \left(\frac{P_7}{P_5}\right) \left(\frac{P_1}{P_8}\right) \left(\frac{P_4}{P_3}\right) \quad (C22)$$

The turbine power can then be calculated by using

$$W_T = \dot{m} C_P T_{in} \eta_T \left[ 1 - \left(\frac{P_{in}}{P_{ex}}\right)^{-(\gamma-1)/\gamma} \right] \quad (C23)$$

With this expression, equation (C21), and the definition of the laser parameter  $N_L$ , the ratio of turbine power to laser output is

$$\frac{W_T}{Q_L} = \frac{\eta_T}{N_L} \left(\frac{T_4}{T_1}\right) \left[ 1 - \left(L_t \frac{P_8}{P_7}\right)^{-(\gamma-1)/\gamma} \right] \quad (C24)$$

In terms of the turbine power and the specified gross shaft output power, the ratio of compressor power to laser output power is

$$\frac{W_C}{Q_L} = \frac{W_T}{Q_L} - \frac{P_{SH}}{Q_L} \quad (C25)$$

The compressor power can also be expressed similar to equation (C6) as

$$\frac{W_C}{Q_L} = \frac{1}{N_L \eta_C} \left(\frac{T_7}{T_1}\right) \left[ \left(\frac{P_8}{P_7}\right)^{(\gamma-1)/\gamma} - 1 \right] \quad (C26)$$

This is solved for the compressor inlet temperature

$$\frac{T_7}{T_1} = \frac{N_L \eta_C \left( \frac{W_C}{Q_L} \right)}{\left( \frac{P_8}{P_7} \right)^{(\gamma-1)/\gamma} - 1} \quad (C27)$$

The turbine exit and compressor exit temperatures are, in terms of  $N_L$ ,

$$T_5 = T_4 - N_L T_1 \left( \frac{W_T}{Q_L} \right) \quad (C28)$$

$$T_8 = T_7 + N_L T_1 \left( \frac{W_C}{Q_L} \right) \quad (C29)$$

The exit temperatures from the lower temperature recuperator are

$$T_6 = T_5 - E_{RL}(T_5 - T_8) \quad (C30)$$

$$T_9 = T_8 + E_{RL}(T_5 - T_8) \quad (C31)$$

The higher temperature recuperator must have the following effectiveness in order to obtain the specified turbine inlet temperature:

$$E_{RH} = \frac{T_3 - T_4}{T_3 - T_9} \quad (C32)$$

The heat-source inlet temperature is then

$$T_{10} = T_9 + (T_3 - T_4) \quad (C33)$$

The thermal efficiency is defined as the sum of laser output power and shaft power divided by the thermal input

$$\eta_{cy} = \frac{Q_L + P_{SH}}{\dot{m}C_P(T_1 - T_{10})} \quad (C34)$$

or in terms of  $N_L$

$$\eta_{cy} = \frac{N_L T_1 \left(1 + \frac{P_{SH}}{Q_L}\right)}{T_1 - T_{10}} \quad (C35)$$

The heat rejection between points 6 and 7 is to the coolant fluid of the radiator loop. The coolant temperatures are

$$T_{7,L} = \frac{1}{E_S} [T_7 - (1 - E_S)T_6] \quad (C36)$$

and

$$T_{6,L} = T_{7,L} + C_R(T_6 - T_7) \quad (C37)$$

The radiator area is then calculated, by using equation (C17), as

$$\frac{A_{R,P}}{Q_L} = \frac{1}{T_1 N_L C_R 4\epsilon_r \sigma T_S^3} \left\{ \ln \left[ \frac{(T_{6,L} - T_S)(T_{7,L} + T_S)}{(T_{7,L} - T_S)(T_{6,L} + T_S)} \right] - 2 \left[ \tan^{-1} \left( \frac{T_{6,L}}{T_S} \right) - \tan^{-1} \left( \frac{T_{7,L}}{T_S} \right) \right] \right\} \quad (C38)$$

The specific prime radiator area is therefore

$$\frac{A_{R,P}}{Q_L + P_{SH}} = \frac{\frac{A_{R,P}}{Q_L}}{1 + \frac{P_{SH}}{Q_L}} \quad (C39)$$

## Electric-Discharge Gas Laser Cycles

Using equation (C5) and the definition of  $N_L$  yields the ratio of compressor power to laser output for the loop configuration A as

$$\frac{W_C}{Q_L} = \frac{1}{\eta_C N_L} \left( \frac{T_2}{T_1} \right) \left[ \left( \frac{1}{L_t} \right)^{(\gamma-1)/\gamma} - 1 \right] \quad (C40)$$

where the reciprocal of the compressor pressure ratio  $L_t$  includes the losses in the laser (eq. (7)) and those in the ducting and heat exchanger. Using equation (6) yields

$$\frac{W_C}{Q_L} = \frac{1}{\eta_C N_L} \left[ 1 + N_L \left( \frac{1 - \eta_E}{\eta_E} \right) \right] \left[ \left( \frac{1}{L_t} \right)^{(\gamma-1)/\gamma} - 1 \right] \quad (C41)$$

The compressor exit temperature is

$$T_3 = T_2 + T_1 N_L \left( \frac{W_C}{Q_L} \right) \quad (C42)$$

Substituting equations (6) and (C41) into equation (C42) yields

$$\frac{T_3}{T_1} = \left[ 1 + N_L \left( \frac{1 - \eta_E}{\eta_E} \right) \right] \left\{ 1 + \frac{1}{\eta_C} \left[ \left( \frac{1}{L_t} \right)^{(\gamma-1)/\gamma} - 1 \right] \right\} \quad (C43)$$

The cycle efficiency is

$$\eta_{cy} = \frac{Q_L}{\frac{Q_E}{\eta_{PS}} + \frac{W_C}{\eta_{PS}}} \quad (C44)$$

where it has been assumed for simplicity that the power system efficiency for supplying the laser electrical input equals that for supplying the compressor power. By using equation (C41) the cycle thermal efficiency can be written

$$\eta_{cy} = \frac{\eta_{PS}}{\frac{1}{\eta_E} + \left\{ \frac{1}{\eta_C N_L} \left[ \left( \frac{1}{L_t} \right)^{(\gamma-1)/\gamma} - 1 \right] \left[ 1 + N_L \left( \frac{1 - \eta_E}{\eta_E} \right) \right] \right\}} \quad (C45)$$

For loop configuration B, the compressor power divided by the laser output is expressed as

$$\frac{W_C}{Q_L} = \frac{1}{\eta_C N_L} \left( \frac{T_3}{T_1} \right) \left[ \left( \frac{1}{L_t} \right)^{(\gamma-1)/\gamma} - 1 \right] \quad (C46)$$

and

$$\frac{W_C}{Q_L} = \frac{1}{N_L} \left( 1 - \frac{T_3}{T_1} \right) \quad (C47)$$

Equating these expressions and solving for  $T_3/T_1$  yields

$$\frac{T_3}{T_1} = \frac{1}{1 + \frac{1}{\eta_C} \left[ \left( \frac{1}{L_t} \right)^{(\gamma-1)/\gamma} - 1 \right]} \quad (C48)$$

The cycle thermal efficiency for loop configuration B is obtained from equations (C44), (C47), and (C48):

$$\eta_{cy} = \frac{\eta_{PS}}{\frac{1}{\eta_E} + \frac{1}{N_L} \left\{ \frac{\frac{1}{\eta_C} \left[ \left( \frac{1}{L_t} \right)^{(\gamma-1)/\gamma} - 1 \right]}{1 + \frac{1}{\eta_C} \left[ \left( \frac{1}{L_t} \right)^{(\gamma-1)/\gamma} - 1 \right]} \right\}} \quad (C49)$$

In both loop configurations the prime specific radiator area for the laser loop is calculated by using equation (C17) and the definition of  $N_L$ . The radiator coolant temperatures at the inlet to and exit from the radiator are

$$T_{L,ex} = \frac{1}{E_S} [T_{G,ex} - (1 - E_S)T_{G,in}] \quad (C50)$$

$$T_{L,in} = T_{L,ex} + C_R(T_{G,in} - T_{G,ex}) \quad (C51)$$

where  $T_{G,in}$  and  $T_{G,ex}$  are the gas temperatures at inlet and exit, respectively, of the heat-source heat exchanger.

The power system radiator area is

$$\frac{(A_{R,P})_{PS}}{Q_L} = \frac{(A_{R,P})_{PS}}{W_C} \left( \frac{W_C}{Q_L} \right) + \frac{(A_{R,P})_{PS}}{Q_E} \left( \frac{1}{\eta_E} \right) \quad (C52)$$

where the power system specific prime radiator areas for compressor work  $(A_{R,P})_{PS}/W_C$  and for laser electrical input  $(A_{R,P})_{PS}/Q_E$  are specified parameters. For simplicity, they are assumed to be equal. They are assigned a reference value (see table III) of  $0.93 \text{ m}^2/\text{kW}$  ( $10 \text{ ft}^2/\text{kW}$ ), which could be achieved with an advanced Brayton system. The total radiator area, the sum of the laser loop radiator area and the power system radiator area, is denoted as  $(A_{R,P})_T/Q_L$ .

## REFERENCES

1. Gerry, Edward T.: Gas Dynamic Laser. *Laser Focus*, vol. 6, no. 12, Dec. 1970, pp. 27-31.
2. Hill, Allan E.: Uniform Electrical Excitation of Large-Volume High-Pressure Near-Sonic CO<sub>2</sub>-N<sub>2</sub>-He Flowstream. *Applied Physics Letters*, vol. 18, no. 5, Mar. 1971, pp. 194-197.
3. Hertzberg, A.; Johnston, E. W.; and Ahlstrom, H. G.: Photon Generators and Engines for Laser Power Transmission. Paper No. 71-106, AIAA, Jan. 1971.
4. Tulip, J.; and Seguin, H.: Gas-Dynamic CO<sub>2</sub> Laser Pumped by Combustion of Hydrocarbons. *Jour. Applied Physics*, vol. 42, no. 9, Aug. 1971, pp. 3393-3401.
5. Hammitt, A. G.: Chemical and Thermal Laser Considered as an Energy Conversion System. *Proceedings of the 6th Intersociety Energy Conversion Engineering Conference*, Boston, Mass., Aug. 3-5, 1971, pp. 761-767.
6. Rich, J. W.; Thompson, H. M.; Treanor, C. E.; and Daiber, J. W.: An Electrically Excited Gas-Dynamic Carbon Monoxide Laser. *Applied Physics Letters*, vol. 19, no. 7, Oct. 1971, pp. 230-232.
7. Wilson, J.: Nitrogen Laser Action in a Supersonic Flow. *Applied Physics Letters*, vol. 8, no. 7, Apr. 1966, pp. 159-161.
8. Anderson, John D., Jr.: Time Dependent Analysis of Population Inversions in an Expanding Gas. *Physics of Fluids*, vol. 13, no. 8, Aug. 1970, pp. 1983-1989.
9. Rigrod, W. W.: Gain Saturation and Output Power of Optical Masers. *Jour. Applied Physics*, vol. 34, no. 9, Sept., 1963, pp. 2602-2609.
10. Lee, George; and Gowen, Forrest E.: Gain of CO<sub>2</sub> Gasdynamic Lasers. *Applied Physics Letters*, vol. 18, no. 6, Mar. 1971, pp. 237-239.
11. Lee, George; Gowen, Forrest E.; and Hagen, Jack R.: Gain and Power of CO<sub>2</sub> Gasdynamic Lasers. *AIAA Jour.*, vol. 10, no. 1, Jan. 1972, pp. 65-71.
12. Kuehn, Donald M.; and Monson, Daryl J.: Experiments with a CO<sub>2</sub> Gas-Dynamic Laser. *Applied Physics Letters*, vol. 16, no. 1, Jan. 1970, pp. 48-50.
13. Anderson, Warren E.; and Wong, Norman D.: Experimental Investigation of a Large-Scale, Two-Dimensional Mixed-Compression Inlet System Performance at Design Conditions,  $M_\infty = 3.0$ . NASA TM X-2016, 1970.
14. Hasel, Lowell E.; and Sinclair, Archibald, R.: A Preliminary Investigation of Methods for Improving the Pressure Recovery Characteristics of Variable Geometry Supersonic-Subsonic Diffuser Systems. NACA RM L57HO2, 1957.

15. Glassman, Arthur J.; and Stewart, Warner L.: Thermodynamic Characteristics of Brayton Cycles for Space Power. Jour. Spacecraft and Rockets, vol. 1, no. 1, Jan. 1964, pp. 25-31.

TABLE I. - PARAMETER REFERENCE VALUES - LASER-COMPRESSOR CYCLE

Gas specific-heat ratio, $\gamma$ . . . . .	1.4
Compressor adiabatic efficiency, $\eta_C$ . . . . .	0.85
Recuperator effectiveness, $E_R$ . . . . .	0.9
Heat-sink heat-exchanger effectiveness, $E_S$ . . . . .	0.9
Capacity rate ratio of heat-sink heat exchanger, $C_R = (\dot{m}C_P)_G / (\dot{m}C_P)_L$ . . . . .	0.85
Sink temperature, $T_S$ , K ( $^{\circ}R$ ) . . . . .	256 (460)
Radiator emissivity, $\epsilon_r$ . . . . .	0.85
Power system efficiency, $\eta_{PS}$ , percent . . . . .	25
Power system specific prime radiator area, $(A_{R,P})_{PS} / W_C$ , $m^2/kW$ ( $ft^2/kW$ ) . . . . .	0.93 (10)

TABLE II. - PARAMETER REFERENCE VALUES - LASER-BRAYTON CYCLE

Gas specific-heat ratio, $\gamma$ . . . . .	1.4
Turbine adiabatic efficiency, $\eta_T$ . . . . .	0.9
Compressor adiabatic efficiency, $\eta_C$ . . . . .	0.85
Recuperator effectiveness (lower temperature), $E_{RL}$ . . . . .	0.9
Heat-sink heat-exchanger effectiveness, $E_S$ . . . . .	0.9
Capacity rate ratio of heat-sink heat exchanger, $C_R = (\dot{m}C_P)_G / (\dot{m}C_P)_L$ . . . . .	0.85
Sink temperature, $T_S$ , K ( $^{\circ}R$ ) . . . . .	256 (460)
Radiator emissivity, $\epsilon_r$ . . . . .	0.85

TABLE III. - PARAMETER REFERENCE VALUES - ELECTRIC-DISCHARGE CYCLE

Gas specific-heat ratio, $\gamma$ . . . . .	1.4
Compressor adiabatic efficiency, $\eta_C$ . . . . .	0.85
Heat-sink heat-exchanger effectiveness, $E_S$ . . . . .	1
Capacity rate ratio of heat-sink heat exchanger, $C_R = (\dot{m}C_P)_G / (\dot{m}C_P)_L$ . . . . .	1
Sink temperature, $T_S$ , K ( $^{\circ}R$ ) . . . . .	256 (460)
Radiator emissivity, $\epsilon_r$ . . . . .	0.85
Power system efficiency, $\eta_{PS}$ , percent . . . . .	25
Power system specific radiator area, $(A_{R,P})_{PS} / W_C$ , $(A_{R,P})_{PS} / Q_E$ , $m^2/kW$ ( $ft^2/kW$ ) . . . . .	0.93 (10)

TABLE IV. - CO<sub>2</sub>-N<sub>2</sub>-He THERMALLY PUMPED GAS DYNAMIC

LASER - PREDICTED PERFORMANCE

[Laser inlet pressure, 30 atm ( $3.0 \times 10^6$  N/m<sup>2</sup>).]

Laser inlet temperature		Nozzle area ratio	Laser output, $Q_L$ , kW	Gas composition mole fraction		Laser performance, $N'_L = Q_L / \dot{m} H_{T_1}$
K	°F			CO <sub>2</sub>	He	
1367	2000	6.0	10	0.03	0.40	0.0011
		6.0	100	.016	.20	.0034
		6.0	1000	.016	.20	.0074
		11.9	10	.04	.20	.0038
		11.9	100	.017	.15	.0066
		11.9	1000	.017	.15	.011
1644	2500	6.0	10	0.05	0.50	0.0040
		6.0	100	.05	.40	.0067
		6.0	1000	.02	.35	.010

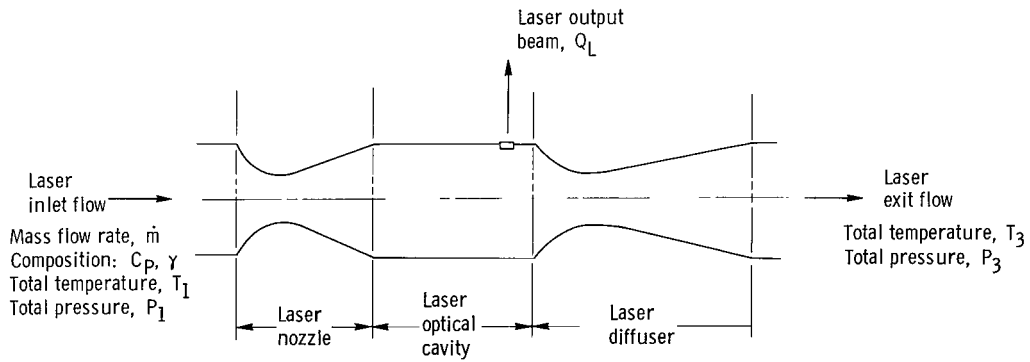


Figure 1. - Schematic of the thermally pumped gas dynamic laser.

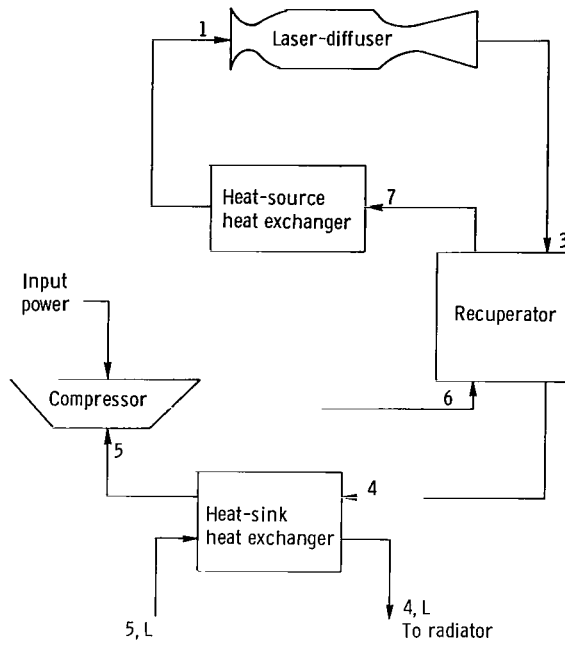


Figure 2. - Schematic of gas dynamic laser-compressor cycle.

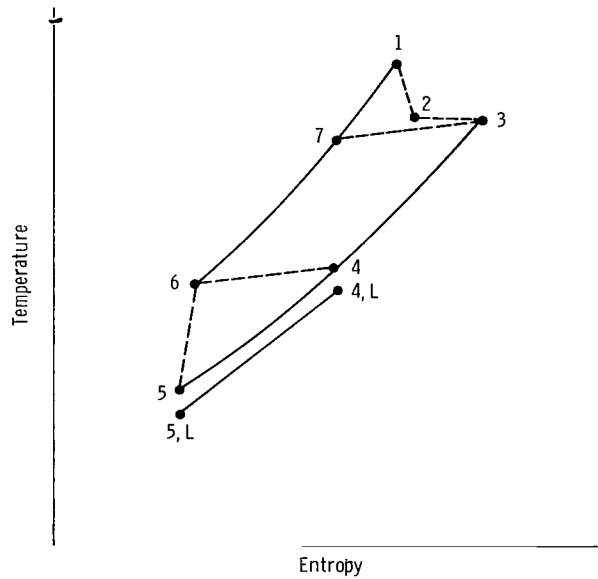


Figure 3. - Temperature-entropy diagram for gas dynamic laser-compressor cycle.

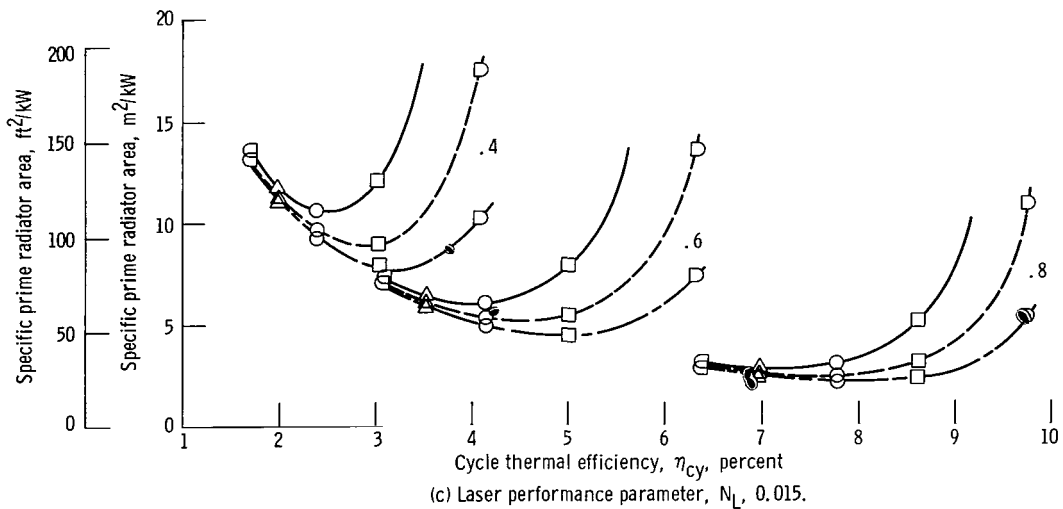
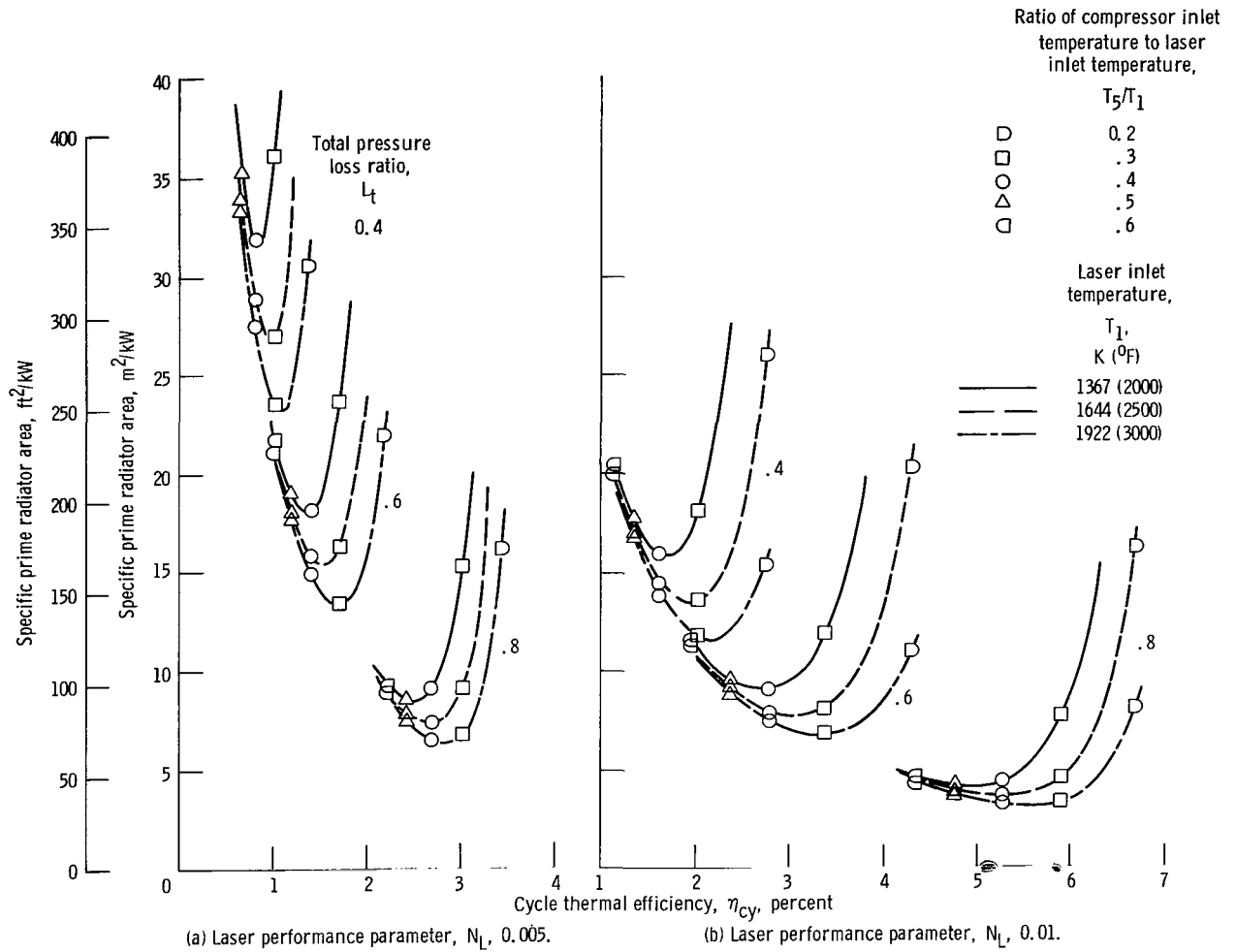


Figure 4. - Effect of total pressure loss ratio and laser performance parameter on laser-compressor cycle.

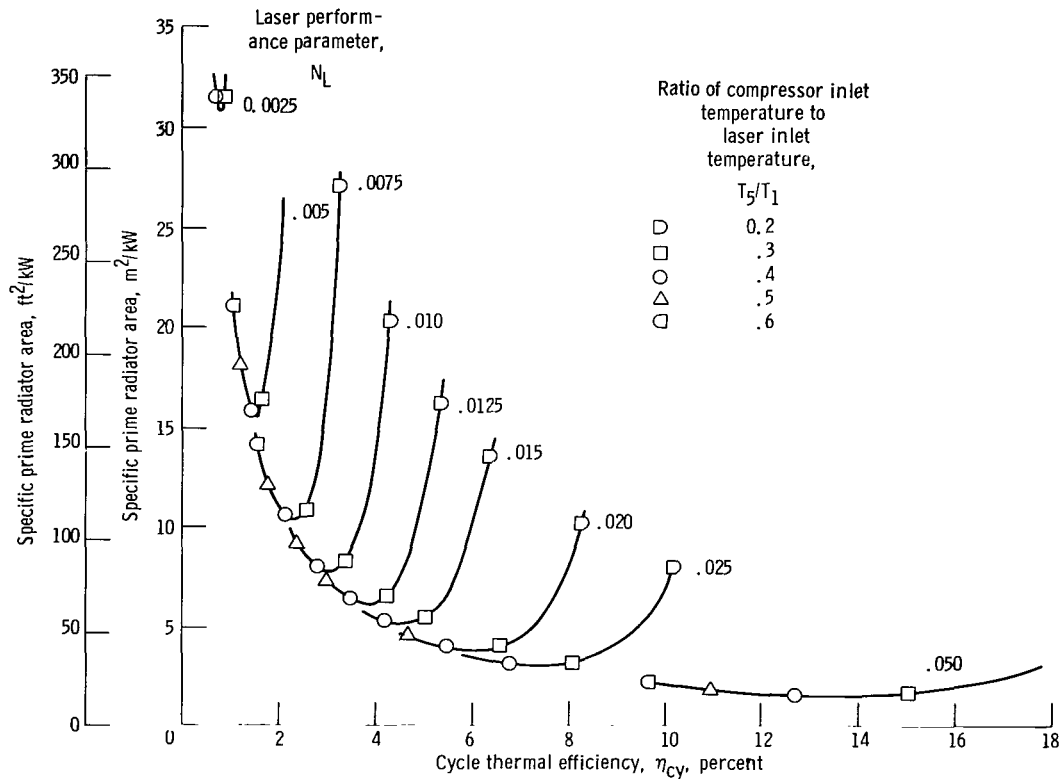


Figure 5. - Effect of laser performance parameter on laser-compressor cycle. Laser inlet temperature, T<sub>1</sub>, 1644 K (2500° F); total pressure loss ratio, L<sub>t</sub>, 0.6.

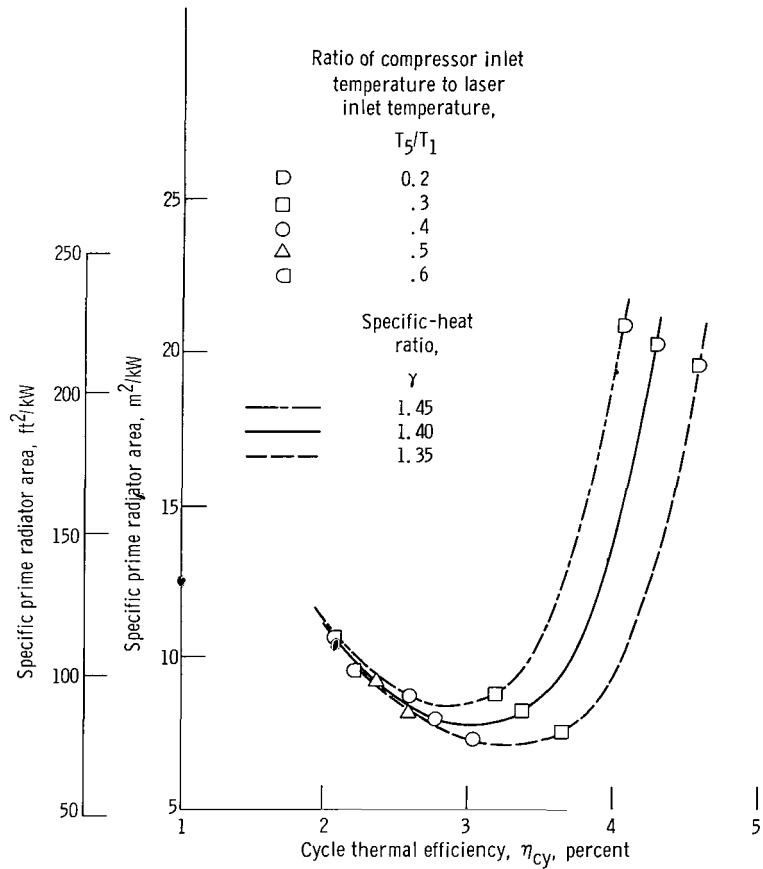


Figure 6. - Effect of specific-heat ratio on laser-compressor cycle. Laser inlet temperature,  $T_1$ , 1644 K (2500° F); laser performance parameter,  $N_L$ , 0.01; total pressure loss ratio,  $L_t$ , 0.6.

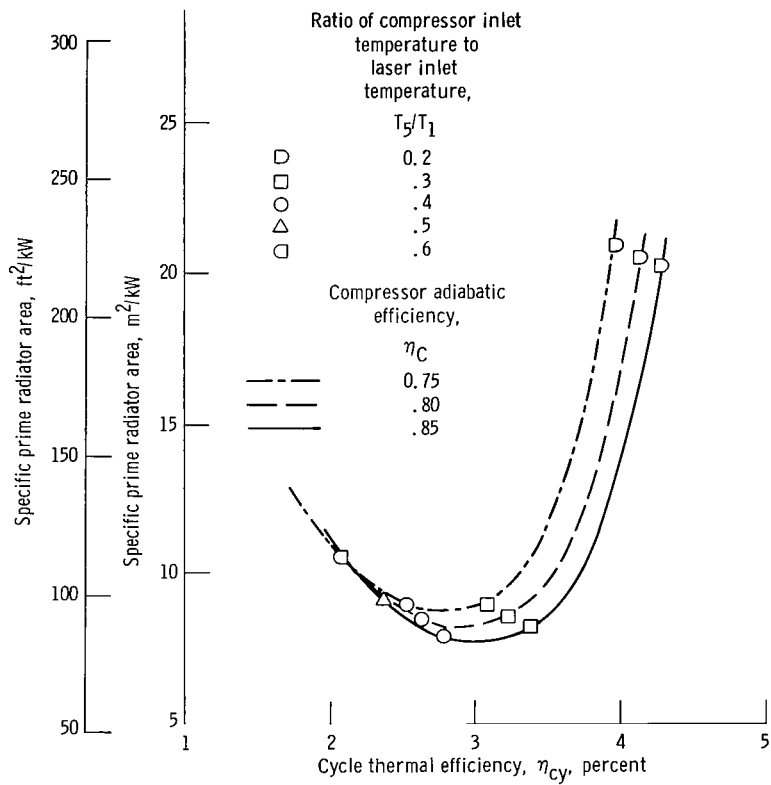


Figure 7. - Effect of compressor adiabatic efficiency on laser-compressor cycle. Laser inlet temperature,  $T_1$ , 1644 K (2500° F); laser performance parameter,  $N_L$ , 0.01; total pressure loss ratio,  $L_t$ , 0.6.

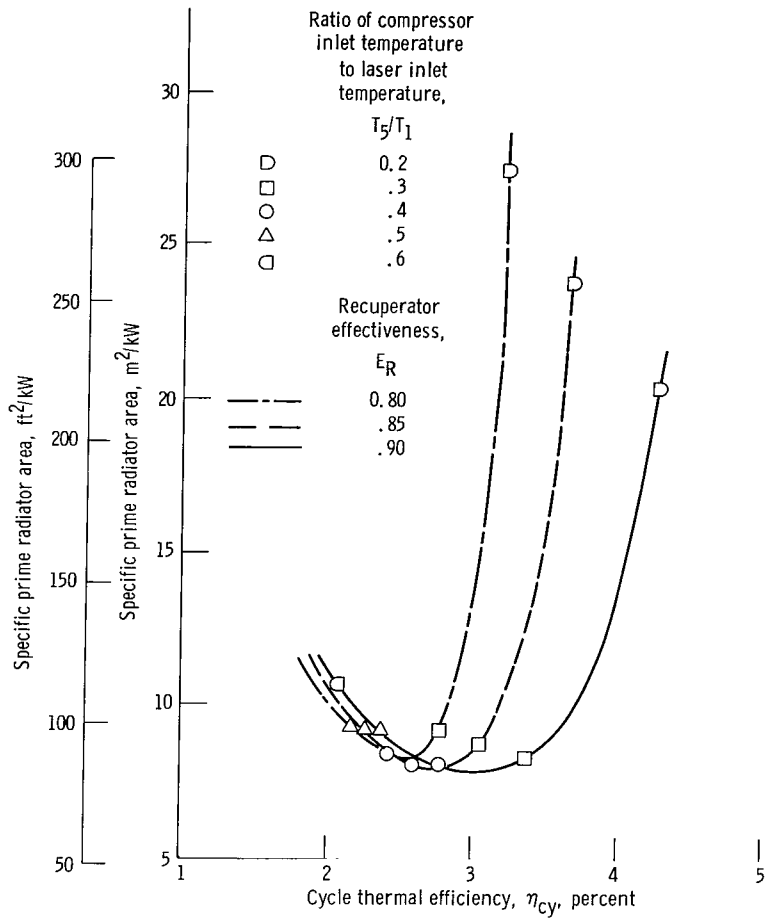


Figure 8. - Effect of recuperator effectiveness on laser-compressor cycle. Laser inlet temperature,  $T_1$ , 1644 K (2500° F); laser performance parameter,  $N_L$ , 0.01; total pressure loss ratio,  $L_t$ , 0.6.

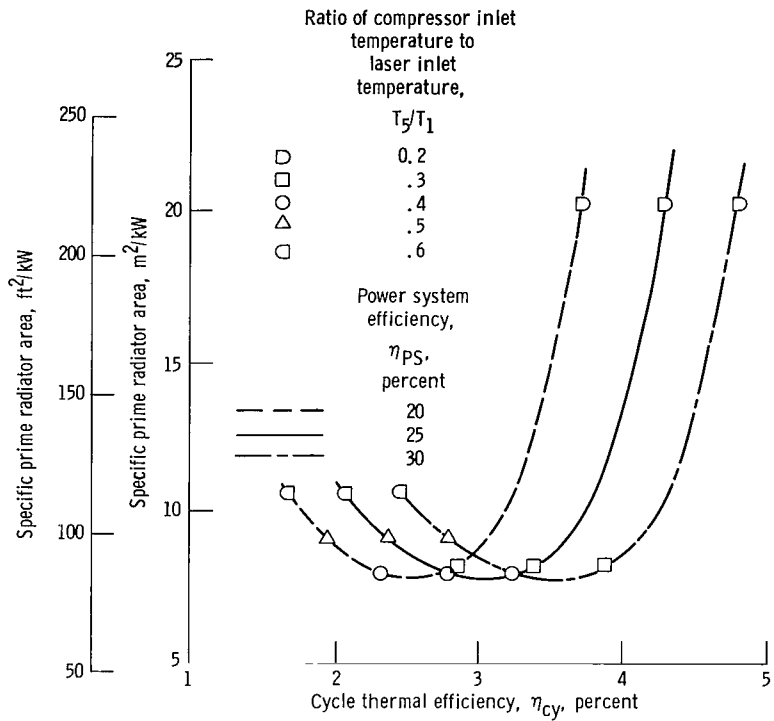


Figure 9. - Effect of power system efficiency on laser-compressor cycle. Laser inlet temperature,  $T_1$ , 1644 K (2500° F); laser performance parameter,  $N_L$ , 0.01; total pressure loss ratio,  $L_t$ , 0.6.

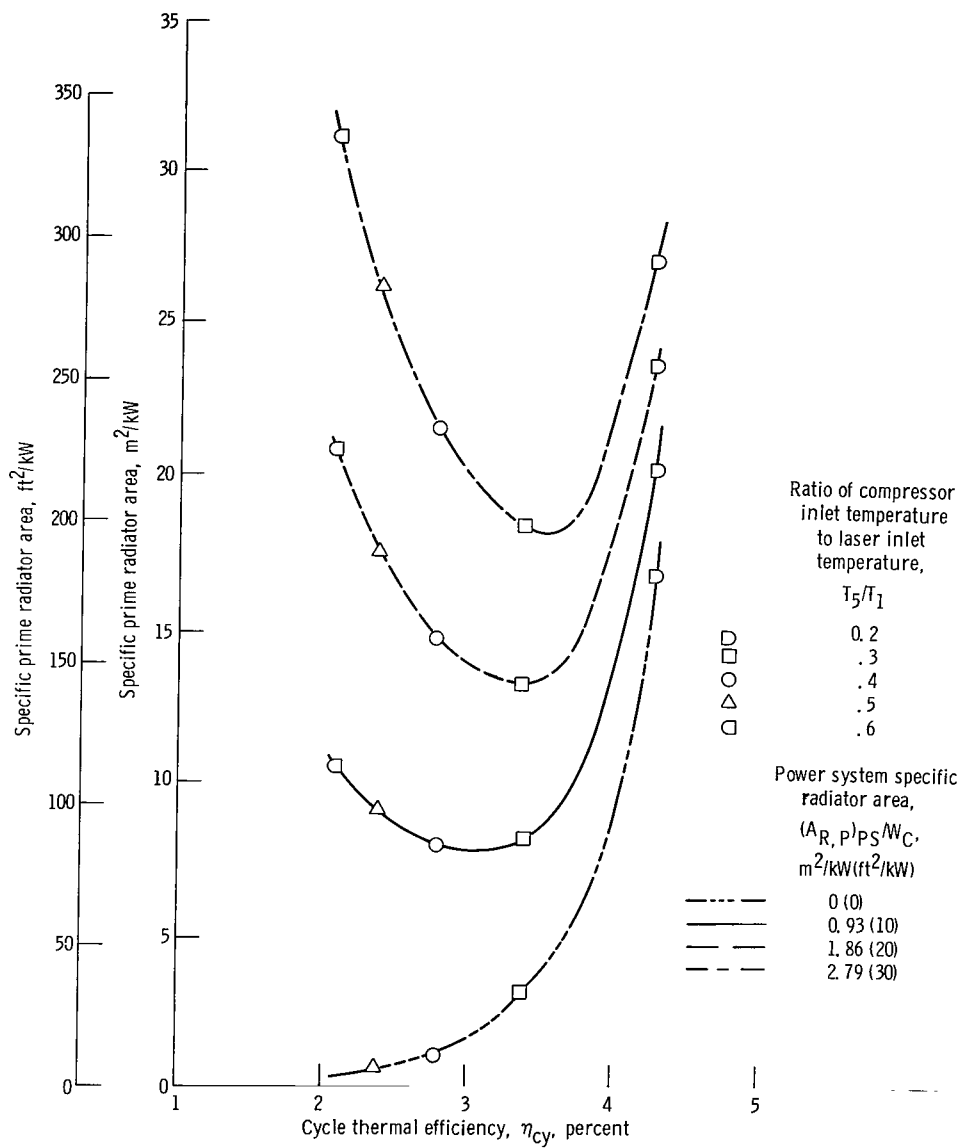
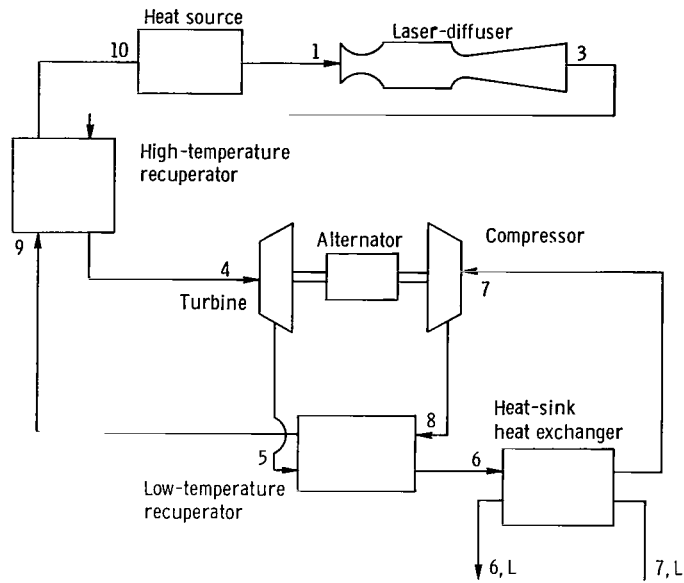
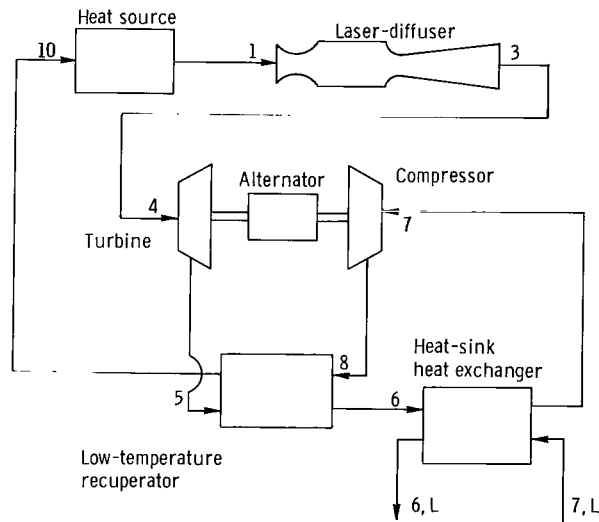


Figure 10. - Effect of power system specific radiator area on laser-compressor cycle. Laser inlet temperature,  $T_1$ , 1644 K (2500° F); laser performance parameter,  $N_L$ , 0.01; total pressure loss ratio,  $L_t$ , 0.6.



(a) Basic laser-Brayton cycle.



(b) Special case of laser-Brayton cycle where turbine inlet temperature is specified to be equal to diffuser exit temperature.

Figure 11. - Schematic of gas dynamic laser-Brayton cycle.

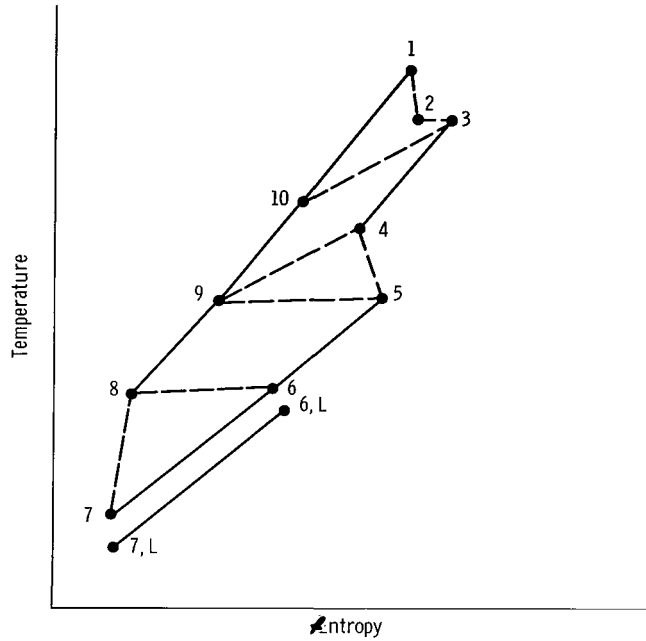


Figure 12. - Temperature-entropy diagram for gas dynamic laser-Brayton cycle.

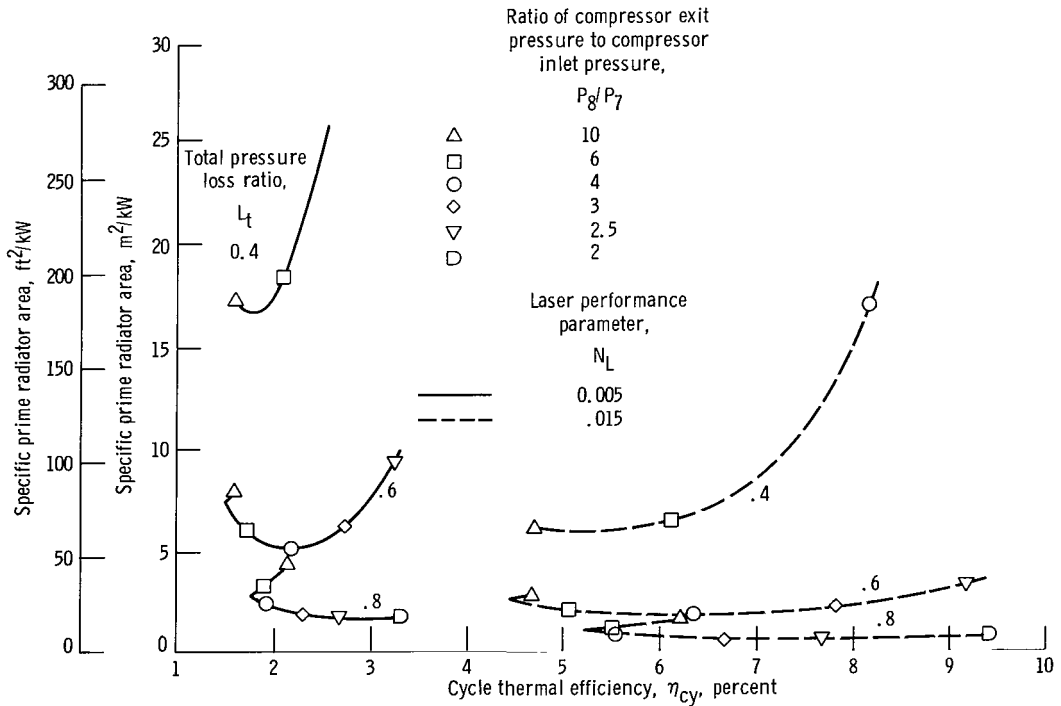


Figure 13. - Effect of total pressure loss ratio and laser performance parameter on laser-Brayton cycle. Gross shaft power,  $P_{SH}$ , 0; laser inlet temperature,  $T_1$ , 1644 K (2500° F); turbine inlet temperature equal to laser exit temperature,  $T_4 = T_3$ .

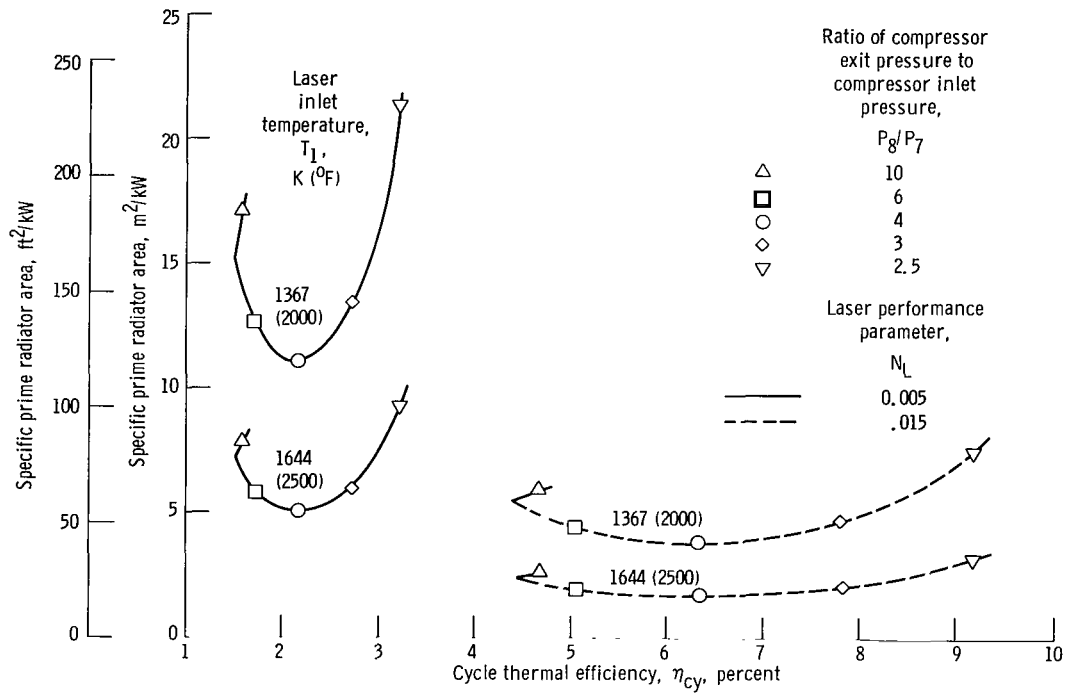


Figure 14. - Effect of laser inlet temperature on laser-Brayton cycle. Gross shaft power,  $P_{SH}$ , 0; total pressure loss ratio,  $L_t$ , 0.6; turbine inlet temperature equal to laser exit temperature,  $T_4 = T_3$ .

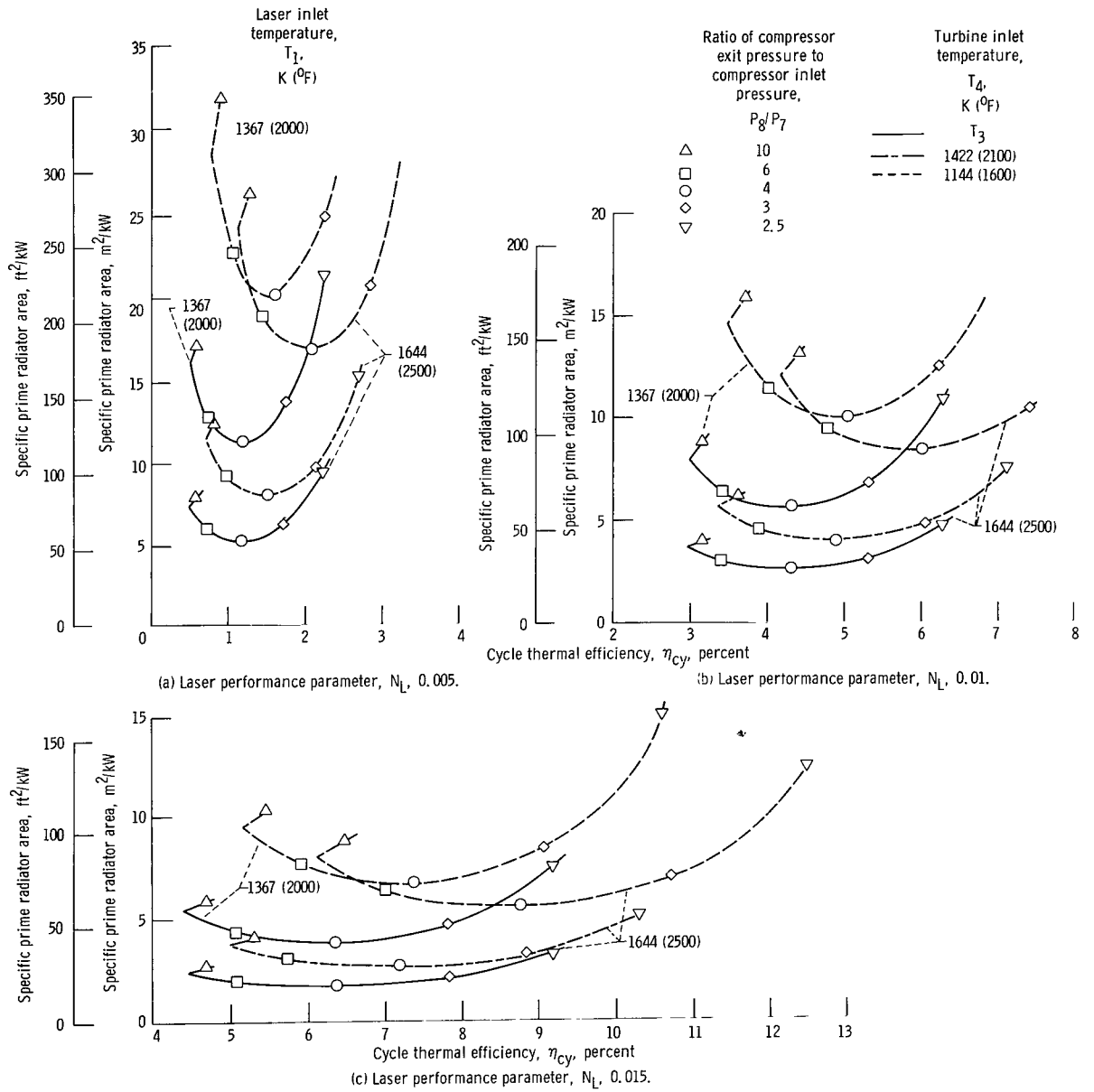


Figure 15. - Effect of turbine inlet temperature on laser-Brayton cycle. Gross shaft power,  $P_{SH}$ , 0; total pressure loss ratio,  $L_t$ , 0.6.

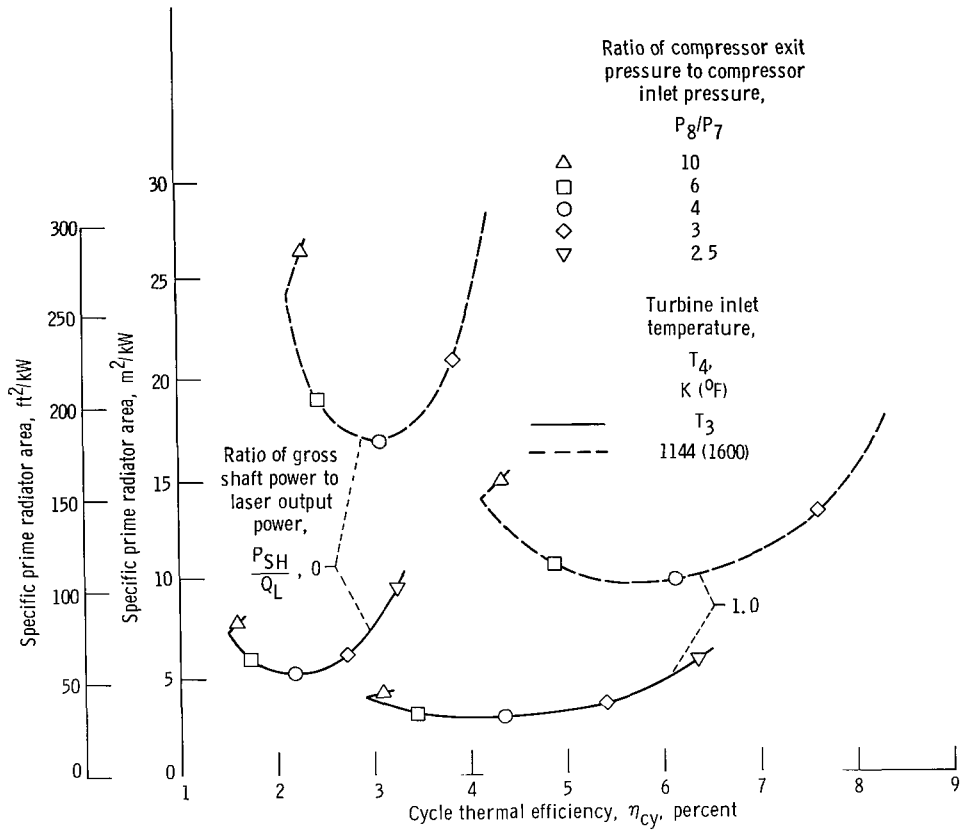


Figure 16. - Effect of gross shaft power on laser-Brayton cycle. Laser inlet temperature,  $T_1$ , 1644 K (2500° F); laser performance parameter,  $N_L$ , 0.005; total pressure loss ratio,  $L_t$ , 0.6.

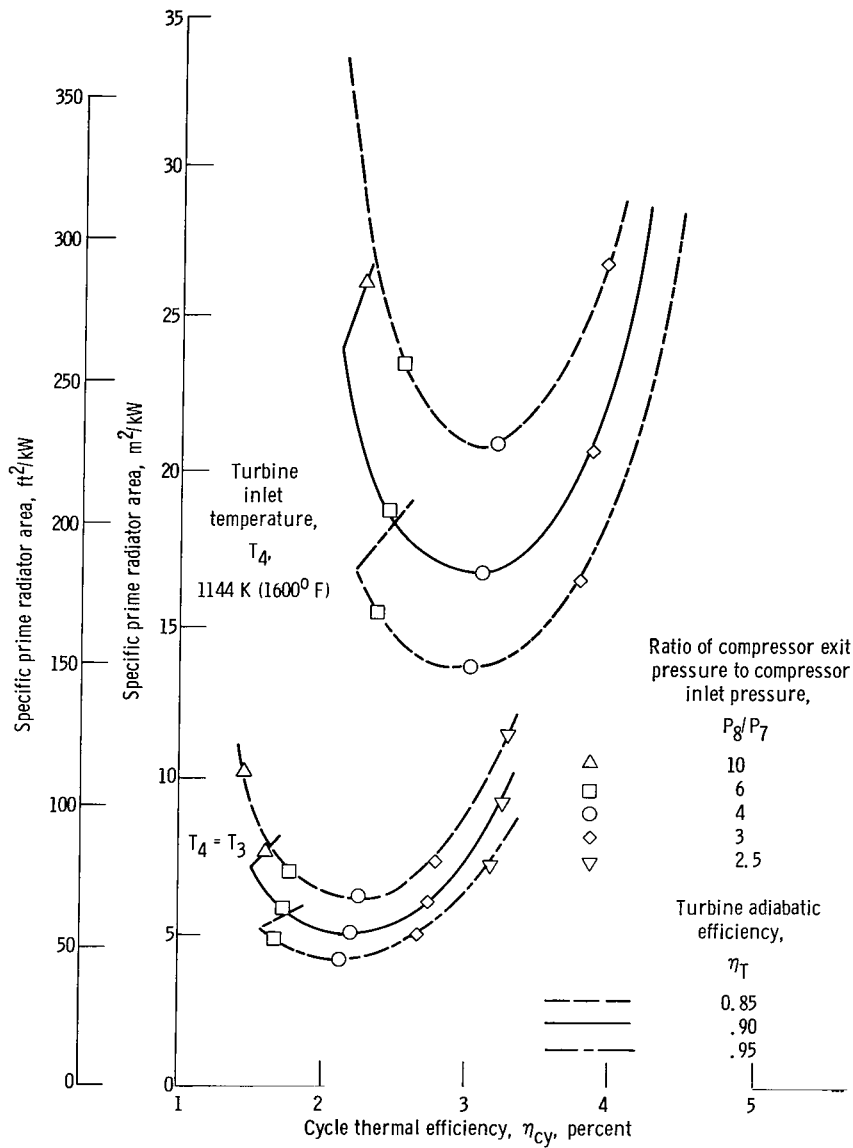


Figure 17. - Effect of turbine efficiency on laser-Brayton cycle. Gross shaft power,  $P_{SH}$ , 0; laser inlet temperature,  $T_1$ , 1644 K (2500° F); laser performance parameter,  $N_L$ , 0.005; total pressure loss ratio,  $L_t$ , 0.6.

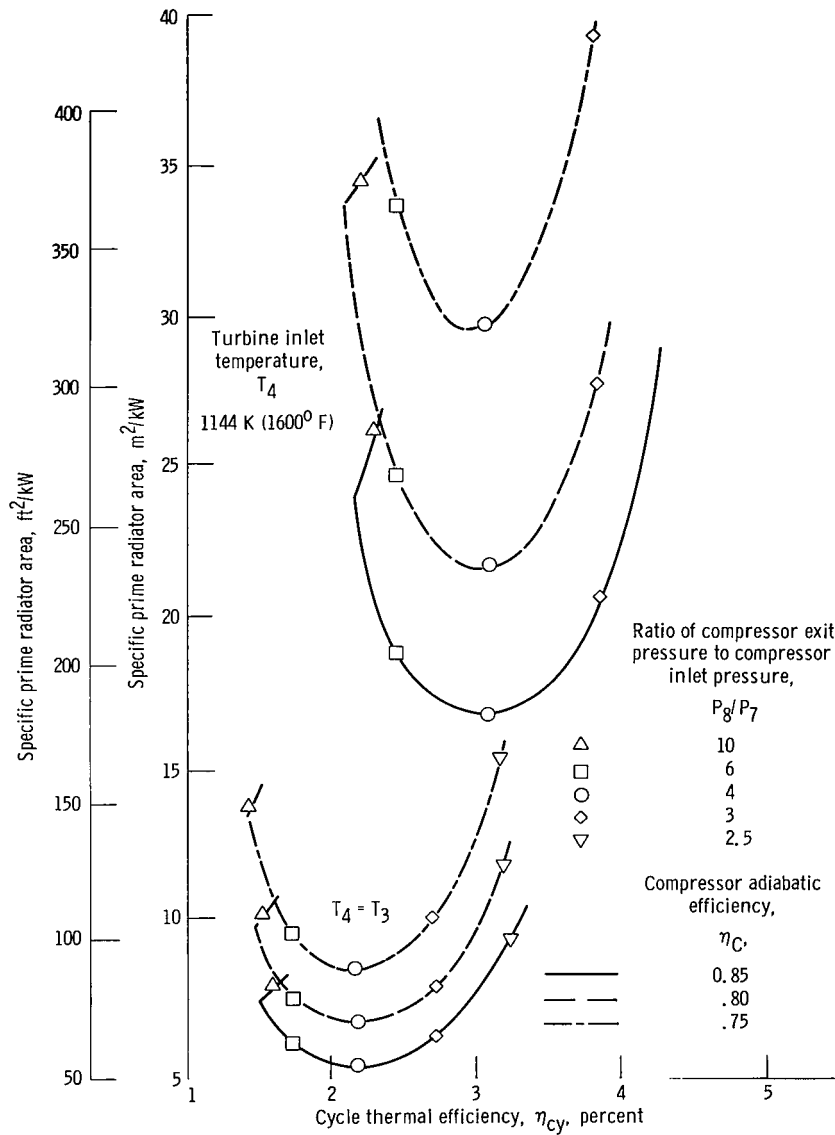


Figure 18. - Effect of compressor efficiency on laser-Brayton cycle. Gross shaft power,  $P_{SH}$ , 0; laser inlet temperature,  $T_1$ , 1644 K (2500° F); laser performance parameter,  $N_L$ , 0.005; total pressure loss ratio,  $L_t$ , 0.6.

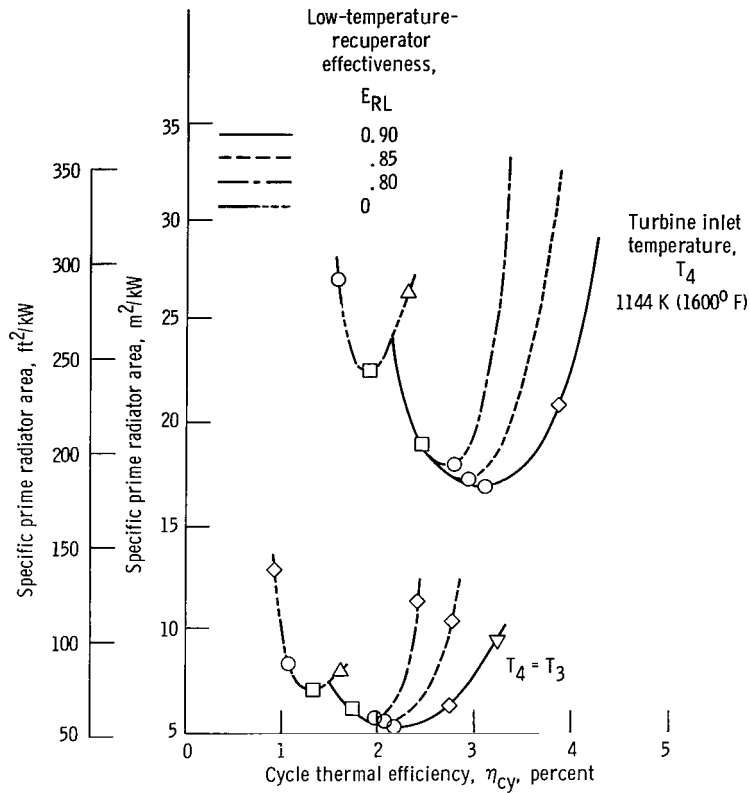


Figure 19. - Effect of low-temperature-recuperator effectiveness on laser-Brayton cycle. Gross shaft power,  $P_{SH}$ , 0; laser inlet temperature,  $T_1$ , 1644 K (2500° F); laser performance parameter,  $N_L$ , 0.005; total pressure loss ratio,  $L_t$ , 0.6.

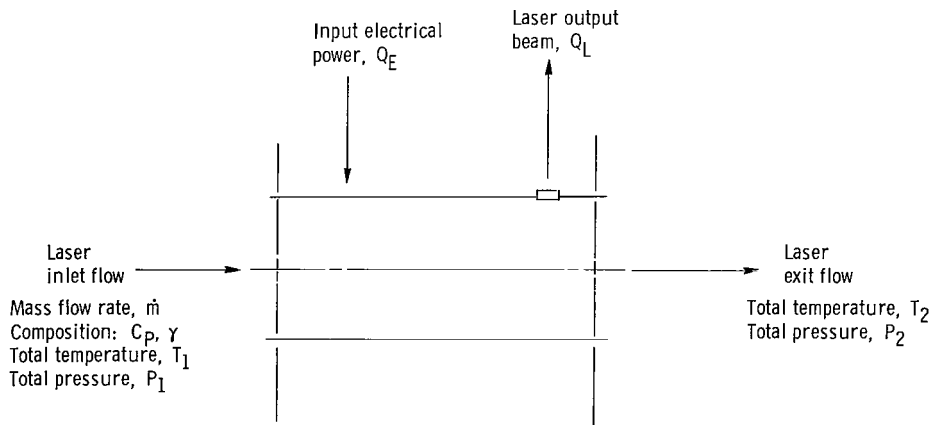
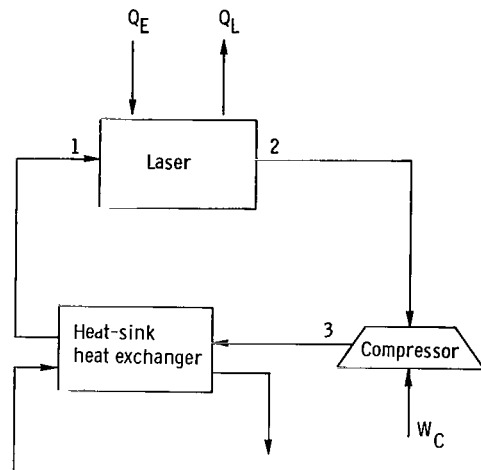
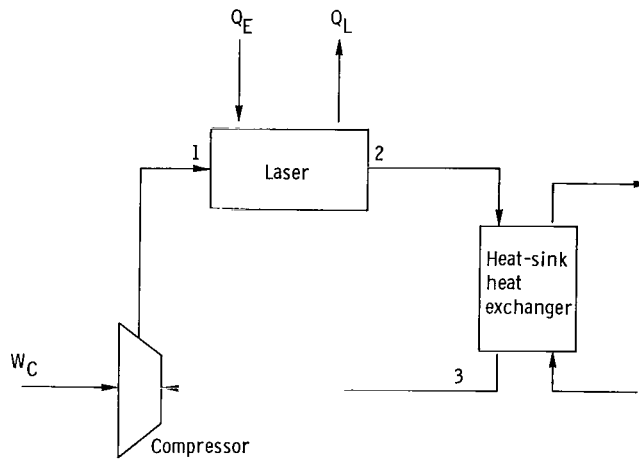


Figure 20. - Schematic of electric-discharge gas laser.



(a) Configuration A.



(b) Configuration B.

Figure 21. - Sketch of electric-discharge laser closed cycle.

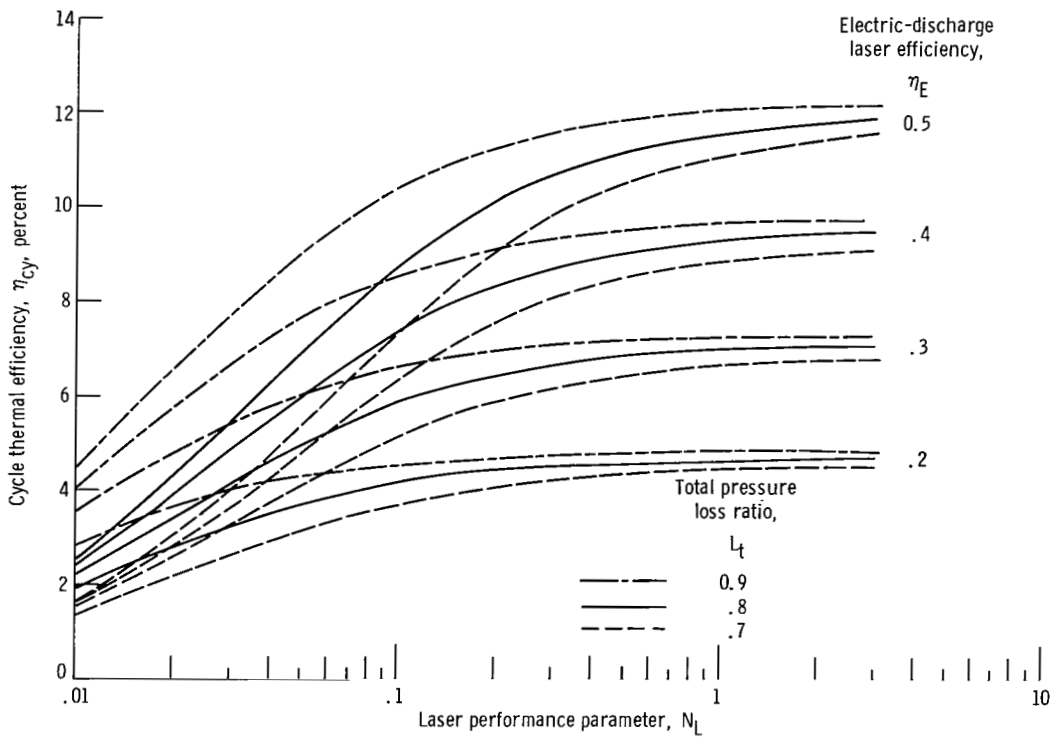


Figure 22. - Cycle efficiency for electric-discharge laser closed-cycle configuration A.

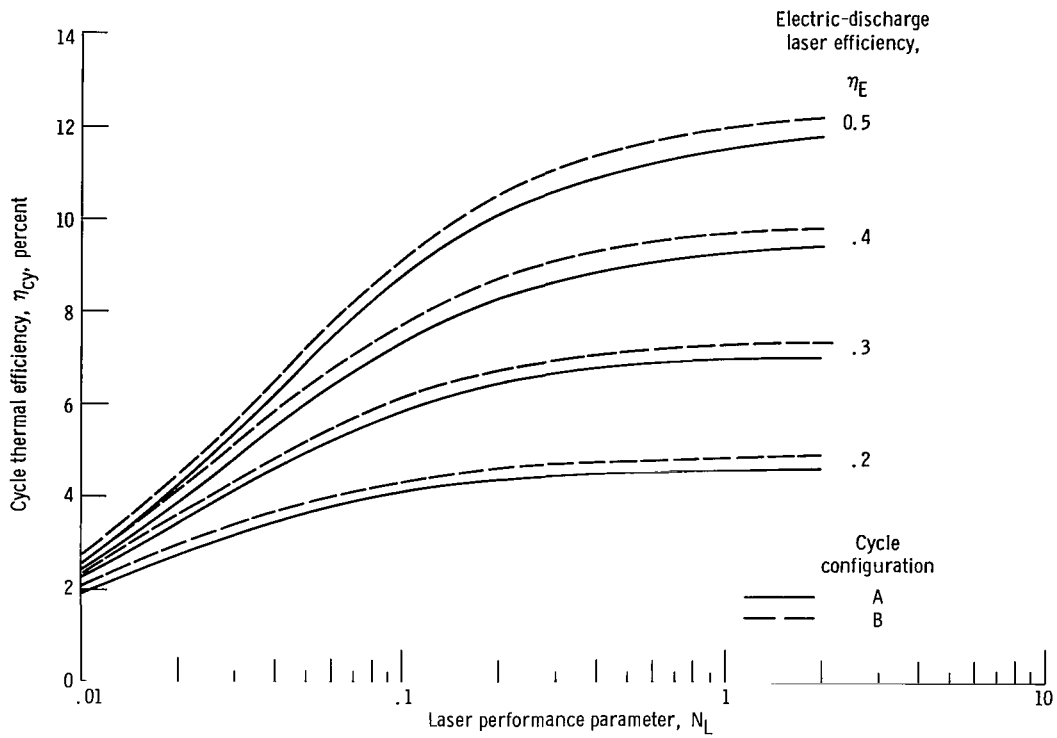


Figure 23. - Comparison of cycle efficiency for electric-discharge laser closed-cycle configurations A and B. Total pressure loss ratio,  $L_t$ , 0.8.

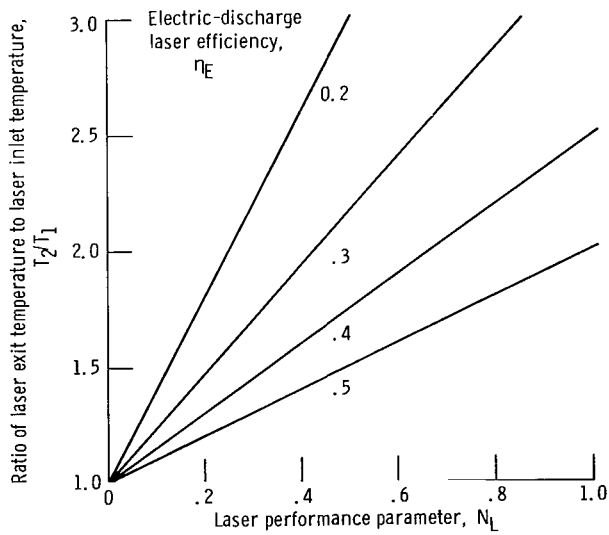


Figure 24. - Laser exit total temperature for electric-discharge laser.

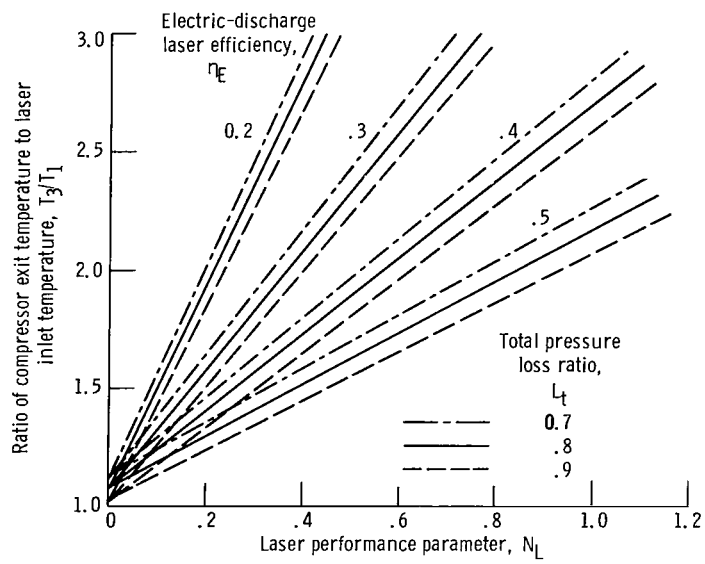


Figure 25. - Compressor exit temperature for electric-discharge laser cycle configuration A.

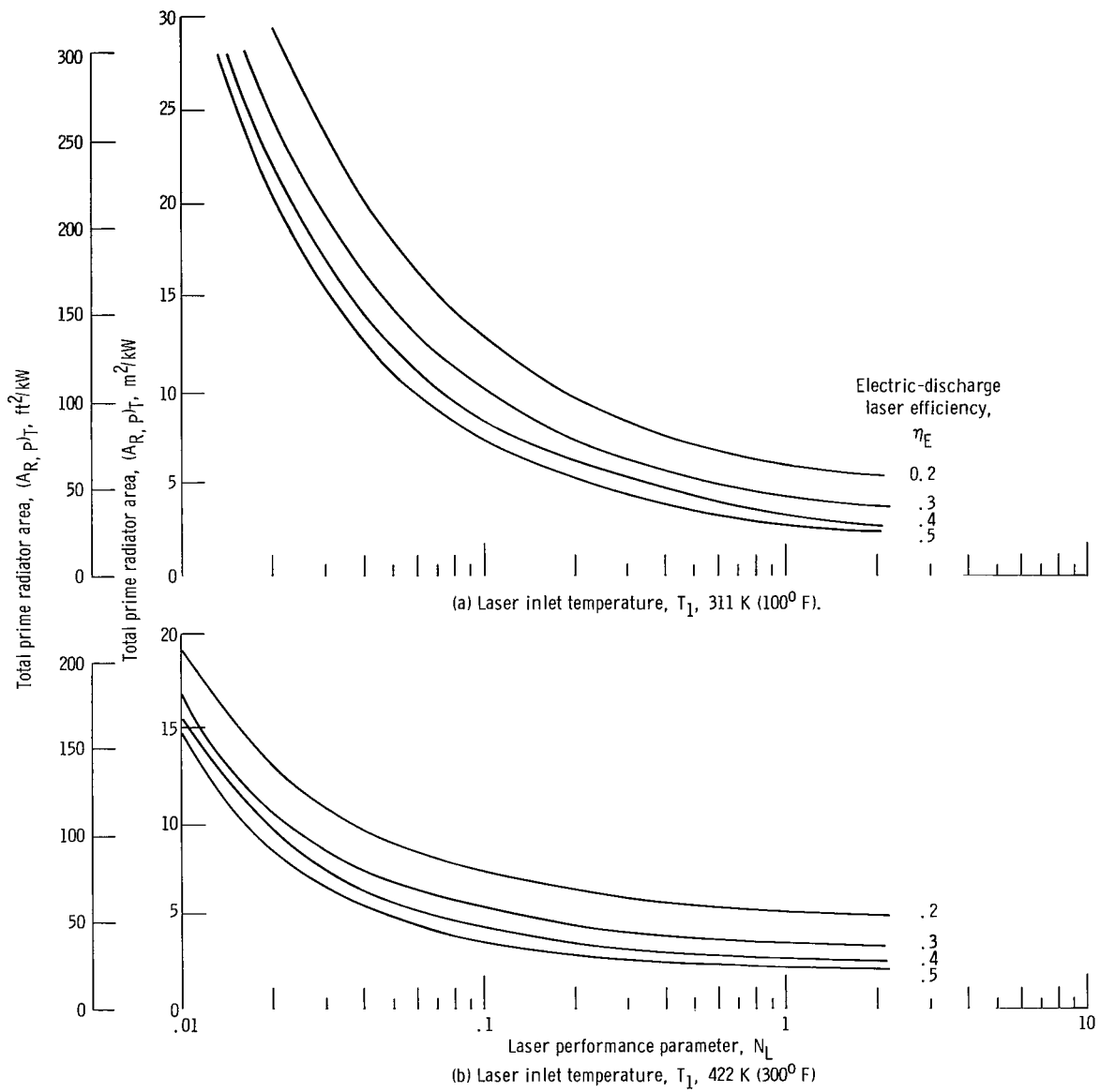


Figure 26. - Total radiator area for electric-discharge laser configuration A. Total pressure loss ratio,  $L_t$ , 0.8.

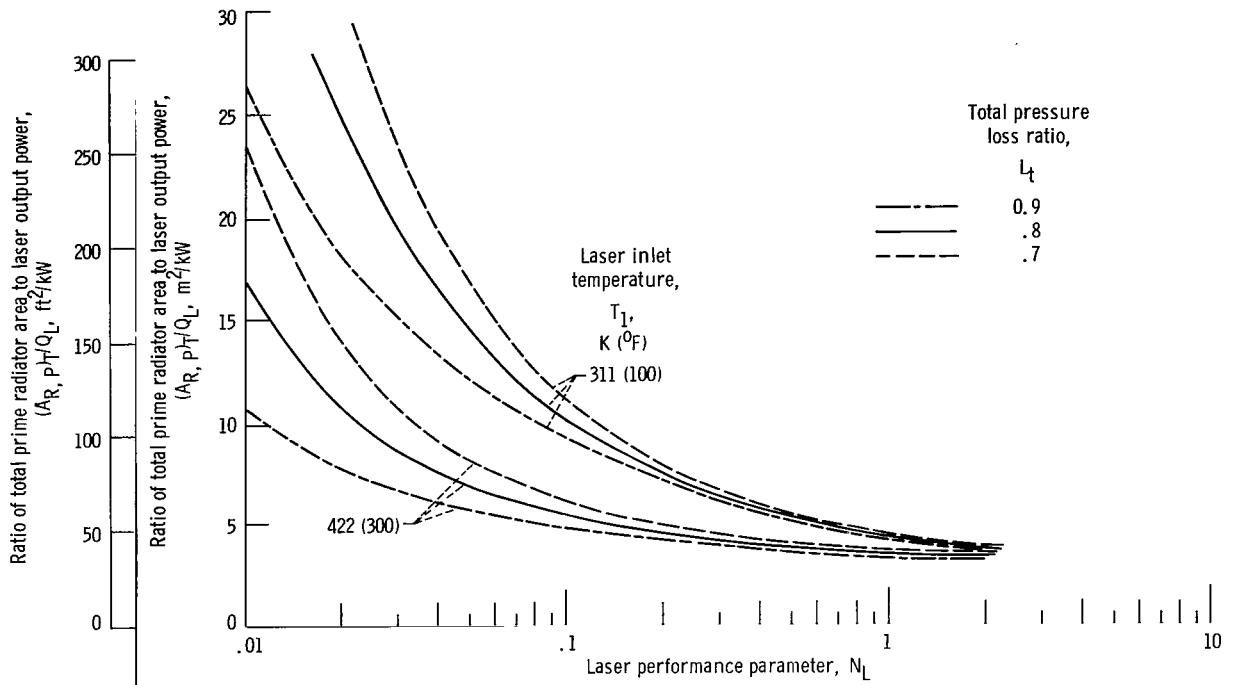


Figure 27. - Effect of total pressure loss ratio on total radiator area for electric-discharge laser configuration A. Electric-discharge laser efficiency,  $\eta_E$ , 0.3.

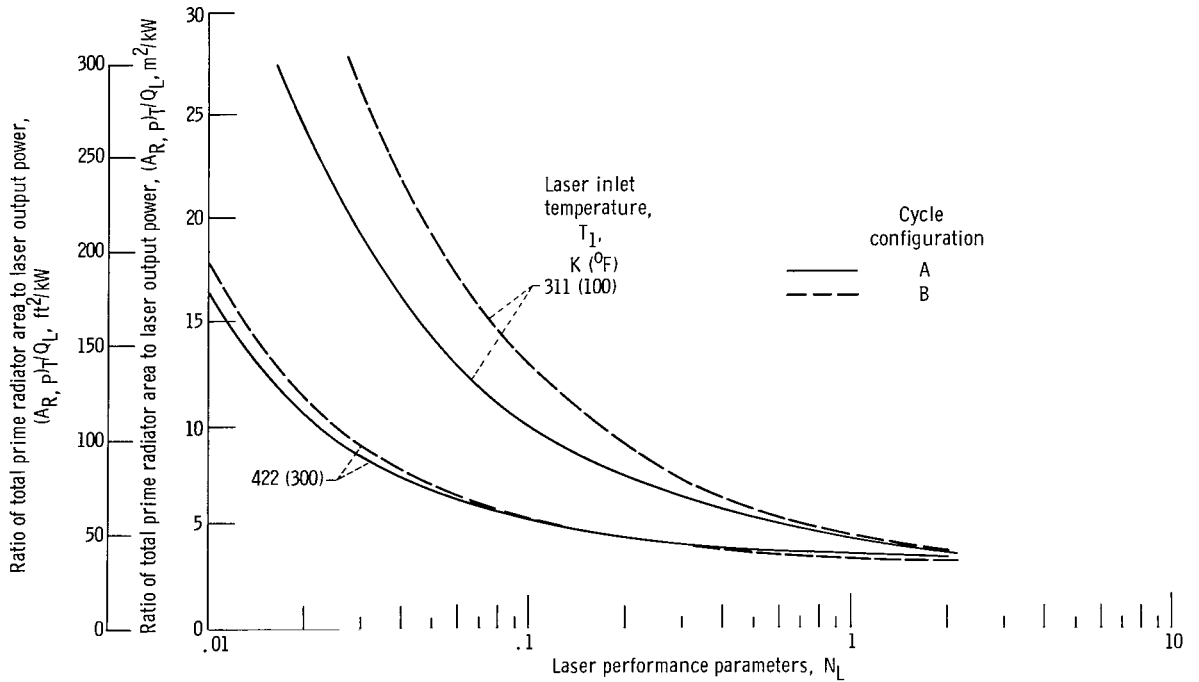


Figure 28. - Comparison of total radiator area for electric-discharge laser configurations A and B. Efficiency,  $\eta_E$ , 0.3; total pressure loss ratio,  $L_t$ , 0.8.

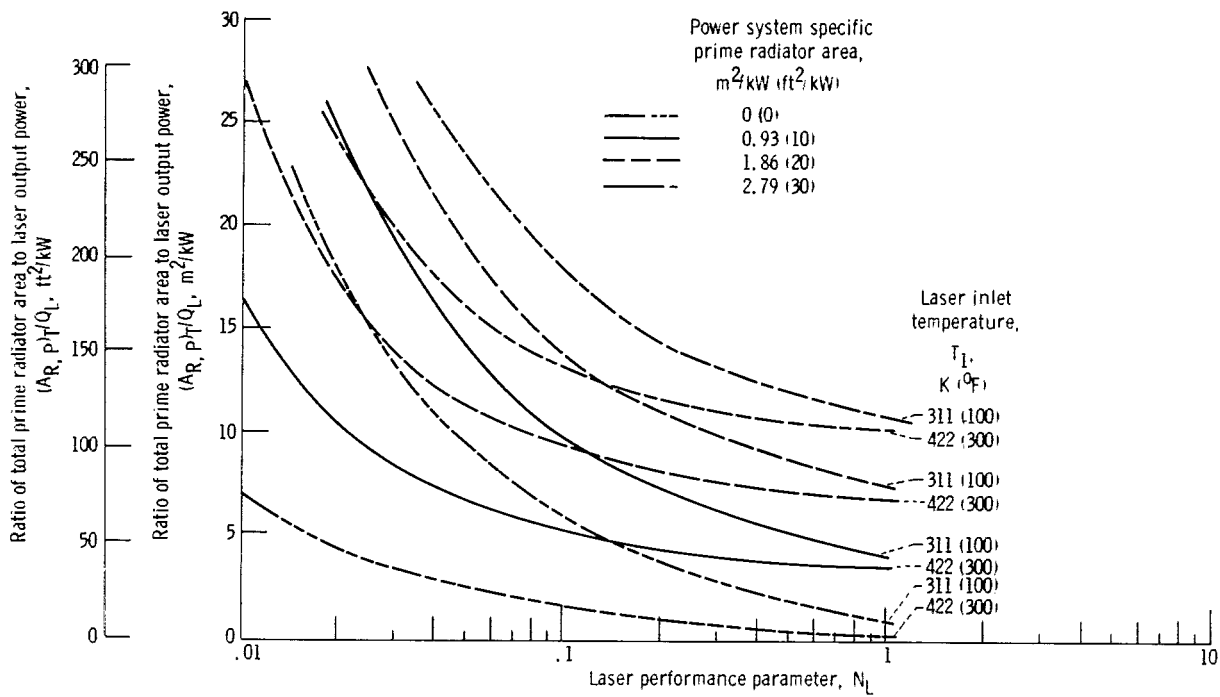


Figure 29. - Effect of power specific radiator area on total radiator area for electric-discharge laser configuration A. Efficiency,  $\eta_E$ , 0.3; total pressure loss ratio,  $L_T$ , 0.8.

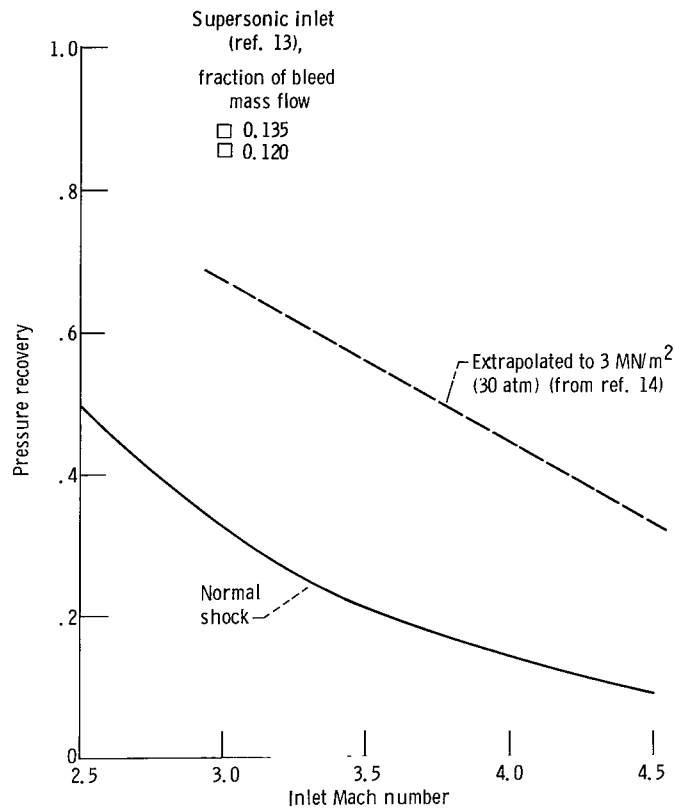


Figure 30. - Total pressure recovery of supersonic diffuser.  
Specific-heat ratio,  $\gamma$ , 1.4.

NATIONAL AERONAUTICS AND SPACE ADMINISTRATION  
WASHINGTON, D.C. 20546

OFFICIAL BUSINESS  
PENALTY FOR PRIVATE USE \$300

SPECIAL FOURTH-CLASS RATE  
BOOK

POSTAGE AND FEES PAID  
NATIONAL AERONAUTICS  
SPACE ADMINISTRATION  
451



POSTMASTER: If Undeliverable (Section 158  
Postal Manual) Do Not Return

*"The aeronautical and space activities of the United States shall be conducted so as to contribute . . . to the expansion of human knowledge of phenomena in the atmosphere and space. The Administration shall provide for the widest practicable and appropriate dissemination of information concerning its activities and the results thereof."*

—NATIONAL AERONAUTICS AND SPACE ACT OF 1958

## NASA SCIENTIFIC AND TECHNICAL PUBLICATIONS

**TECHNICAL REPORTS:** Scientific and technical information considered important, complete, and a lasting contribution to existing knowledge.

**TECHNICAL NOTES:** Information less broad in scope but nevertheless of importance as a contribution to existing knowledge.

**TECHNICAL MEMORANDUMS:** Information receiving limited distribution because of preliminary data, security classification, or other reasons. Also includes conference proceedings with either limited or unlimited distribution.

**CONTRACTOR REPORTS:** Scientific and technical information generated under a NASA contract or grant and considered an important contribution to existing knowledge.

**TECHNICAL TRANSLATIONS:** Information published in a foreign language considered to merit NASA distribution in English.

**SPECIAL PUBLICATIONS:** Information derived from or of value to NASA activities. Publications include final reports of major projects, monographs, data compilations, handbooks, sourcebooks, and special bibliographies.

**TECHNOLOGY UTILIZATION PUBLICATIONS:** Information on technology used by NASA that may be of particular interest in commercial and other non-aerospace applications. Publications include Tech Briefs, Technology Utilization Reports and Technology Surveys.

*Details on the availability of these publications may be obtained from:*

**SCIENTIFIC AND TECHNICAL INFORMATION OFFICE**

**NATIONAL AERONAUTICS AND SPACE ADMINISTRATION**

**Washington, D.C. 20546**